frontiers | Frontiers in Geochemistry

TYPE Original Research
PUBLISHED 08 March 2023
DOI 10.3389/fgeoc.2023.1080169

OPEN ACCESS

EDITED BY
Masaharu Tsuji,
Asahikawa College, Japan

REVIEWED BY
Genming Luo,
China University of Geosciences Wuhan, China
Dongjie Tang,
China University of Geosciences, China

*CORRESPONDENCE
Carlos Herdocia,
cherd002@fiu.edu

SPECIALTY SECTION
This article was submitted to Biogeochemistry, a section of the journal Frontiers in Geochemistry

RECEIVED 25 October 2022
ACCEPTED 02 February 2023
PUBLISHED 08 March 2023

CITATION
Herdocia C and Maurrasse FJ-MR (2023), Geochemical factors associated with deposition of lower Aptian organic-rich sediments during OAE1a in the Basque-Cantabrian Basin, northern Spain. *Front. Geochem.* 1:1080169. doi: 10.3389/fgeoc.2023.1080169

Geochemical factors associated with deposition of lower Aptian organic-rich sediments during OAE1a in the Basque-Cantabrian Basin, northern Spain

Carlos Herdocia* and Florentin J-M. R. Maurrasse

Department of Earth and Environment, Florida International University, Miami, FL, United States

Introduction: The Early Aptian Oceanic Anoxic Event 1a (OAE1a) is characterized by organic matter (OM) bearing rocks identified worldwide, which also occur in the hemipelagic succession of the Cuchía section, North Basque-Cantabrian Basin (NBCB) in Northern Spain. Previous works identified OAE1a using $\delta^{13}C$ calibrated with biostratigraphy of planktonic foraminifera, calcareous nannoplankton, and ammonites. However, the geochemical characteristics that controlled OM sources and the redox conditions during OAE1a are yet to be determined. Therefore, here we present the results of a high-resolution complementary study along 67 m of the succession at Playa de los Caballos beach that highlights how local factors in the basin modulated the effects of increased precipitation during enhanced global hydrological cycles.

Methods: Samples were analyzed for total inorganic carbon (TIC), total organic carbon (TOC), $\delta^{13}C$, major elements (Al, Ti, Si), redox sensitive trace elements (RSTEs), clay mineralogy, bulk mineralogy, and biomarkers.

Results and Discussion: Carbon isotope segments C2 to C6 were recognized to determine the age of the outcrop. Lipid biomarkers indicated that OM is predominantly marine with significant terrestrial contribution. Terrigenous OM was carried to the basin through pulses of fluvial input as attested by the major elements and by high relative proportions of quartz, feldspar, and clay minerals. Increased terrestrial inputs also enhanced primary production and facilitated OM preservation. Periods with hightened RSTE content correspond with increases in the major elements, thus implying their common provenance. High sedimentation rates together with the presence of less labile OM and the interaction with clay minerals most likely played a major role in preserving the OM. This study further highlights how enhanced hydrological cycles significantly influenced the marine conditions that controlled the expression of OAE1a in the NBCB.

KEYWORDS

OAE1a, organic matter, terrigenous contribution, RSTEs, dysoxic

1 Introduction

The Cretaceous System archived periodic alterations of the global carbon cycle that profoundly affected the marine environment. Worldwide coeval sedimentary deposits reveal that these events coincide with extensive greenhouse conditions and severe oxygen deficiency in the ocean termed oceanic anoxic events (OAEs) (Schlanger and Jenkyns, 1976; Arthur et al., 1990). These Cretaceous anoxic events are well documented since the Valanginian (e.g., Lini et al., 1992; Aguirre-Urreta et al., 2008) through the Santonian (Wagreich, 2012). Such an event is widely recognized as OAE1a which characterizes lower Aptian sediments (e.g., Schlanger and Jenkyns, 1976; Arthur, 1979; Arthur et al., 1990; Koutsoukos et al., 1991a; Koutsoukos et al., 1991b; Kuhnt et al., 1998; Masse and Machhour, 1998; Menegatti et al., 1998; Mutterlose and Böckel, 1998; Scarparo Cunha and Koutsoukos, 1998; Larson and Erba, 1999; Maurrasse and Ponton, 2005; Coccioni et al., 2006; Abu-Zied, 2007; Barragán and Maurrasse, 2008; Michalík et al., 2008; Yilmaz, 2008; Moreno-Bedmar et al., 2009; Moreno-Bedmar, 2010; Föllmi, 2012; Husinec et al., 2012; Léonide et al., 2012; Roban and Melinte-Dobrinescu, 2012; Elkhazri et al., 2013; Gaona-Narvaez et al., 2013; Sanchez-Hernandez and Maurrasse, 2014; Socorro and Maurrasse, 2019; Hu et al., 2020; Socorro and Maurrasse, 2020; Herdocia and Maurrasse, 2022; Socorro and Maurrasse, 2022). These studies (herein above) generally agree that different marine physiographic conditions may respond with varieties of facies during OAEs exclusive of black shales and with remarkable differences in degrees of oxygen depletion which may not show OM-rich sediments. Non-etheless, the most important characteristic signature, regardless of the facies, is the distinctive geochemical footprint left in sedimentary deposits coeval with OAE1a as a strong negative carbon isotopic excursion (CIE) archived in both the organic carbon ($\delta^{13}C_{org}$) and in the marine carbonate ($\delta^{13}C_{carb}$) (e.g., Menegatti et al., 1998; Li et al., 2008; Sanchez-Hernandez and Maurrasse, 2016) as well as in lake deposits (Zhang et al., 2016). The pronounced negative shift has been postulated to relate to volcanogenic CO_2 fluxes associated with submarine volcanism (Sinton and Duncan, 1997; Leckie et al., 2002; Tejada et al., 2009) and the emplacement of several large igneous provinces (LIPs), namely, the giant Ontong Java-Manihiki-Hikurangi plateau (125–120 Ma) (Larson, 1991; Tarduno et al., 1991; Tatsumi et al., 1998; Larson and Erba, 1999; Tejada et al., 2009). Thus, this disruption of the global carbon cycle is widely considered to originate from high atmospheric CO_2 that led to strong greenhouse conditions causing a weakened latitudinal temperature gradient (Barron and Washington, 1985; Larson, 1991; Barron et al., 1995; Fletcher et al., 2008). These conditions caused eustatic sea level rise (Haq et al., 1988) and increased the rate of precipitation, weathering, and overland erosion (Bellanca et al., 2002). Hence, these prevalent climatic conditions led to more nutrient supplies that intensified primary productivity, oceanic water column stratification, and episodic expansion of the oxygen minimum zone (Mutterlose and Böckel, 1998; Sanchez-Hernandez and Maurrasse, 2014). Thus, low oxygen in the water column reduced remineralization of OM while heightened burial due to increased terrigenous fluxes led to enhanced preservation of organic matter. These periodic disruptions were especially well developed in semi-restricted and restricted basins (Erbacher and Thurow, 1997; Sanchez-Hernandez and Maurrasse, 2014; Basilone et al., 2017), but they also affected shallower water settings (Najarro et al., 2011a; Gaona-Narvaez et al., 2013). The Lower Aptian in Cantabria, northern Spain (Figure 1A), includes a well-exposed section at Playa de los Caballos, Cuchía (Figures 1B,C), where previous works reported the presence of OAE1a (Figure 1C) (Wilmsen, 2005; Najarro et al., 2011a; Najarro et al., 2011b; García-Mondéjar et al., 2015a; García-Mondéjar et al., 2015b). These earlier studies indicate that overall, the early Aptian evolution of the North Basque-Cantabrian Basin (NBCB) accumulated sediments under various environmental conditions (Najarro et al., 2011a; Najarro et al., 2011b).

Fossil content in the Patrocinio Formation includes ammonites, belemnites, planktonic foraminifera and calcareous nannoplankton. This unit is assigned an early Aptian age and is interpreted as a record of an intraplatform prodelta environment coincident with OAE1a (~120.5 Ma) based on biostratigraphy and the $\delta^{13}C$ curve in two sections: Cuchía and La Florida (Najarro et al., 2011b). The Cuchía section is equal to the interval of OAE1a based on correlation of the carbon isotope chemostratigraphy that can be associated with segments C2 to C7 (Menegatti et al., 1998) along with various biostratigraphic data (Millán et al., 2009; Najarro et al., 2011b; García-Mondéjar et al., 2015b).

The section at Playa de los Caballos (Figures 1B,C) is exceptionally well exposed, and the interval that includes OAE1a shows no noticeable tectonic disturbance; therefore, it provides a reliable archive of the geochemical record associated with the paleoenvironmental response of the NBCB during OAE1a. Given the abrupt facies change associated with the onset of the Patrocinio Fm reported in the previous studies (*op. cit*), further characterization of the biogeochemical processes and the redox conditions that developed during OAE1a remain to be fully addressed in this part of the NBCB, as such information will further clarify our understanding on the controlling geochemical processes of carbon sequestration associated with OAEs. Here we aim at providing additional geochemical data using molecular biomarkers and redox sensitive trace elements (RSTEs) to elucidate the interdependence of the global factors with regards to the NBCB. Thus, the primary objective of the present study is to complement previous works through a comprehensive geochemical analysis focusing on the biogeochemical changes, sources of OM and further characterize the carbon isotope curve of the section. The results provide a better understanding of the local response of the NBCB to the controlling mechanisms of the global carbon sequestration event.

2 Geologic setting

The studied section is in the Northern Province of Cantabria (N Spain) along the Playa de los Caballos beach, near the town of Cuchía (Figures 1A,B). This sedimentary sequence is a component of the NBCB, which is part of the broader Basque-Cantabrian Basin (BCB). The development of the BCB was influenced by the same tectonics related to the opening of the Bay of Biscay through several rifting phases during the Mesozoic-Early Cenozoic which led to the formation of several intra-shelf sub-basins (Choukroune et al., 1973; Puigdefàbregas and Souquet, 1986; Dinarès-Turell and García-Senz,

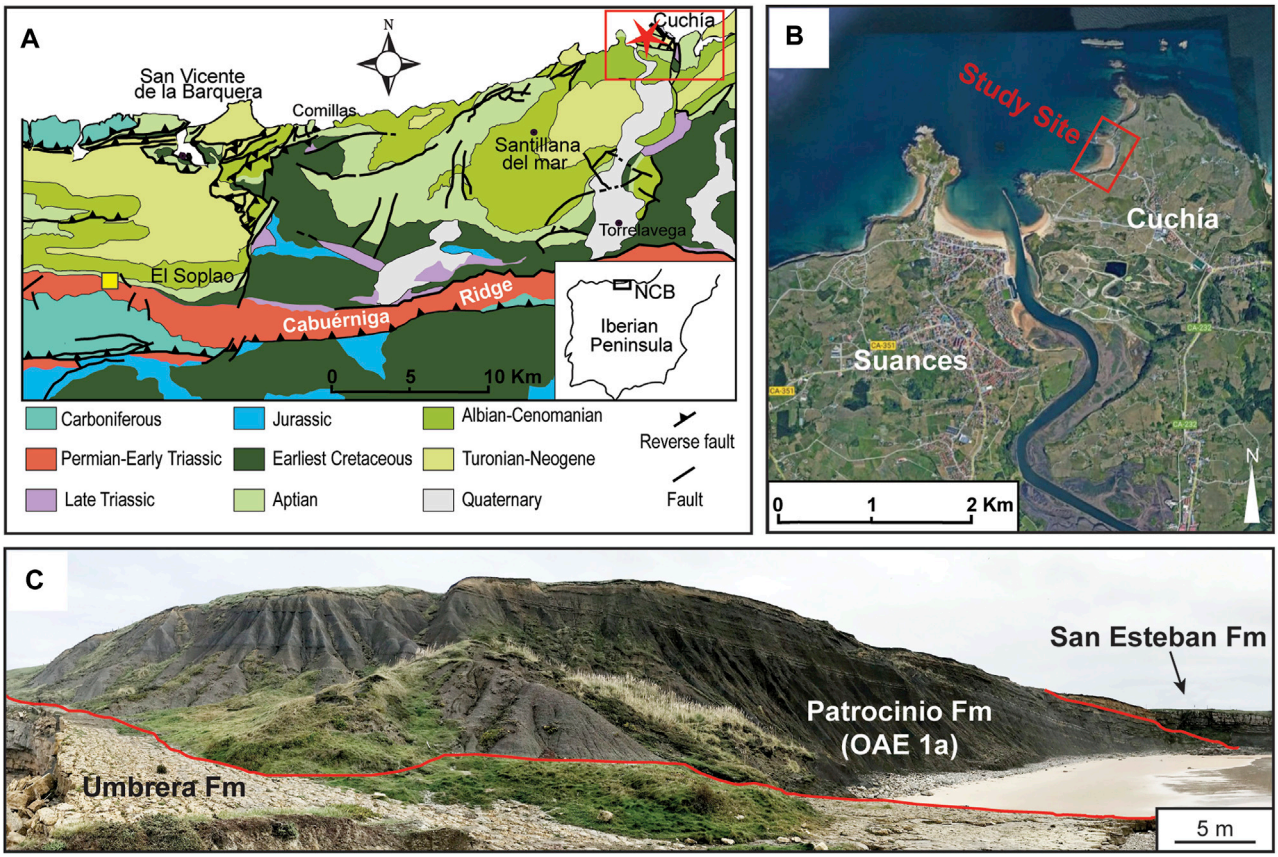

FIGURE 1
(A) Simplified geologic map of the North Basque-Cantabrian Basin (modified after Schlagintweit et al., 2016) with the study location shown in red box with red star and the yellow square represents the Puentenansa/La Florida section (Najarro et al., 2011b; Quijano et al., 2012). **(B)** Arial view of the study site (red square) and the nearby town of Cuchía (taken from Google Earth Pro 2022). **(C)** Panoramic view of the study site showing the three formations (Umbrera, Patrocinio, and San Esteban).

2000; Capote et al., 2002; García-Senz, 2002; Gong et al., 2009; Mencos et al., 2010). The Cuchía section accumulated in one of the sub-basins of the NCB as an E-W elongated extensional depression in the northern part of the BCB (Figure 1A). The NCB was separated from the rest of the more rapidly subsiding BCB by different entities: to the east by the Rio Miera Flexure, a N-S extensional structure; to the south by the Cabuerniga Ridge, an E-W oriented horst structure; to the west by the Asturian Massif; and to the north by the Liencres High, and ENE-WSW oriented swell (Rat, 1988; Martin-Chivelet et al., 2002; Wilmsen, 2005).

Earlier studies (Wilmsen, 2005; Najarro et al., 2011a; Najarro et al., 2011b; García-Mondéjar et al., 2015a; García-Mondéjar et al., 2015b) indicate that the sedimentary sequence at Playa de los Caballos (Figure 1C) spans from the Jurassic to the Cenomanian and includes over 100 m of well-exposed lower Aptian (Figure 2) composed of both terrigenous and carbonate sediments subdivided into 3 units: 1) The lower unit, or the Umbrera Formation, consists of mixed carbonate-siliciclastic and cross-bedded moderate pale orange (10 YR 8/4) bioclastic-oolitic limestones containing hermatypic corals and rudist bivalves. It is interpreted to represent tide influenced, shallow water, high-energy platform deposits which were interrupted by an apparent emergence, then further submergence with a restricted marine environment. 2) The subsequent deposits, designated the Patrocinio Formation, show an abrupt change to medium dark gray (N4), OM-rich silty marlstones and grayish black (N2), soft clayey marlstones with occasional orbitolinid-rich marlstones. This succession of shale, calcareous shale, and marlstone shows an upward increase in siltstone and mica together with bioturbated sandstones that display subaqueous flow structures. 3) Conditions shifted further to open marine associated with delta progradation on a carbonate platform and these deposits are defined as the San Esteban Formation containing orbitolinid-rich, sandy, coral-rudist limestones (Najarro et al., 2011b; García-Mondéjar et al., 2015a). Our study covers the 67 m succession that includes the uppermost part of the Umbrera Formation and most of the Patrocinio Formation associated with OAE1a (Figure 1C; Figure 2).

3 Methods

3.1 Field sampling

The field campaign at Playa de los Caballos (Figure 1C) was conducted in November 2017 and Eighty-three (83) samples were

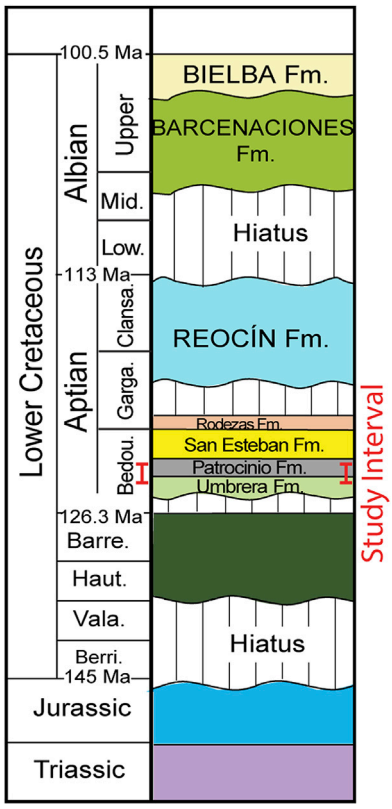

FIGURE 2
Lithostratigraphy of the lower cretaceous in the north Basque-cantabrian basin (modified after Schlagintweit et al., 2016 and from Najarro et al., 2011b).

collected at the nominal Cuchía Section, starting from the uppermost beds of the Umbrera Fm to the middle portion of the Patrocinio Fm, including the entire black shale unit previously reported to correspond to OAE1a (Wilmsen, 2005; Najarro et al., 2011b; García-Mondéjar et al., 2015a; García-Mondéjar et al., 2015b). The sampling resolution is ~0.82 m with slightly closer intervals that target more indurated interbeds. Because of active mass wasting along the outcrop, extra care was given to the sampling process by removing ~5—8 cm of the exposed surface to avoid contamination. Colors assigned to the rocks on dry samples follow the standard "Rock-color chart" of the Geological Society of America (Goddard et al., 1984). The studied portion of the section includes essentially ~2.36 m of limestone layers (medium greenish gray 5GY 5/1) at the base, and the remainder overlying 65.64 m is in sharp contrast consisting of dark shales (greenish black 5GY 2/1) with interbeds of calcareous shales and marlstones (dark greenish gray 5GY 4/1).

3.2 Carbon analysis

The total carbon (TC), total inorganic carbon (TIC), and total organic carbon (TOC) content were measured for all 83 samples at Florida International University (FIU). The analysis was conducted using a LECO CR-412 carbon analyzer following the procedures laid out by Sanchez-Hernandez and Maurrasse (2014). A pure calcite standard reference material (C64-500, Fisher Scientific) was used to calibrate the instrument by producing a best-fit calibration curve. In preparation for the analysis, all samples were powdered using a Bell-Art micromill with a tungsten-carbide chamber and blade. TC content was acquired by introducing approximately 0.3 g of powdered sample to the carbon analyzer. For TIC, before processing the samples with the carbon analyzer, ~0.3 g of powder for each sample was first placed in a muffle furnace at 560 °C for 2 h to remove the organic carbon content. The results produced by the instrument are reported as $CaCO_3$ wt%. Therefore, to obtain TOC as C wt%, the following formula was used: $TOC_{Cwt\%} = (TC - TIC) \times 8.33$, where the 8.33 comes from the molecular weight of $CaCO_3$ divided by the molecular weight of C (100.086/12.011) (Ponton Guerrero, 2006). Here, TIC values are used to assign a lithologic classification based on the nomenclature after Sanchez-Hernandez and Maurrasse (2014), where: limestone, >65% $CaCO_3$; marly-limestone, 60%–65% $CaCO_3$; marlstone, 30%–60% $CaCO_3$; calcareous shale, 10%–30% $CaCO_3$; and shale, 0%–10% $CaCO_3$.

The stable carbon isotope on the organic fraction ($\delta^{13}C_{org}$) was conducted at the Stable Isotope Laboratory (SIL) at FIU using a Thermo Delta C EA-IRMS following the procedures after Swart et al. (2019). Prior to the analysis, powdered samples were decarbonated by acidification with 10% HCl until all the carbonate was removed, then rinsed with deionized (DI) water to raise the pH. The reproducibility of the $\delta^{13}C_{org}$ values is ±0.1‰ based on glycine standards. The results for the $\delta^{13}C_{org}$ are given in per mil (‰) relative to the Vienna Peedee Belemnite standard.

3.3 Major, biolimiting, and redox sensitive trace elements

Elemental analyses were carried out on thirty (30) samples targeting the various lithologies throughout the studied interval of the studied outcrop. Major (Al, Ti, Si), biolimiting (Fe, P), and redox sensitive trace elements (RSTEs; V, Cr, Ni, Mo, U) were analyzed at FIU's Trace Evidence Analysis Facility (TEAF) following the methodology developed by Arroyo et al. (2009). In preparation for the analysis 1.000 g of powdered material were spiked with two internal standard solutions: 300 µl indium metal (1,000 ppm in 3% HNO_3) and 350 µl scandium oxide (1,000 ppm in 3% HNO_3) and set to dry on a heating block at 80 °C for 48 h. Next, samples were further powdered and homogenized using a tungsten carbide ball-mill for 30 min and pressed into pellets ready for analysis. Concentrations were determined by Laser Ablation-Inductively Coupled Mass Spectrometry (LA-ICP-MS) using the ELAN DRCII (Perkin Elmer LAS) with quadrupole in standard operating mode. An LSX-500 with a compact Nd:YAG laser (266 nm) operating with a 200 µm spot size at 10 Hz was used for the ablations. Standard reference materials PACS-2, a marine sediment (National Research Council of Canada, Ottawa, Canada); and two soil reference materials: SRM NIST2710 (Montana Soil) and NIST2704 (Buffalo River Sediment) were used for calibration and to check for accuracy. Results were averaged for each sample

based on five ablations relative to their standard deviations using the GLITTER software. The overall average precision for the analysis was <5% (1.7%–14%) relative standard deviation, with a 0.2% average error based on replicate standards. Major and bioessential elements are reported in mg/g and RSTEs are reported as parts per million (ppm).

3.4 Clay and bulk mineralogy analysis

The clay and mineralogical contents were measured for nine samples (n = 9) using X-ray diffraction (XRD) at the Illinois State Geological Survey, Geochemistry Section, Prairie Research Institute, University of Illinois. The clays were analyzed on the <2 μm fraction to determine the variations of smectite, illite, kaolinite, and chlorite to the basin. The analyses were performed using a Scintag® XDS2000 diffractometer. Sample preparations followed the procedures laid out by Moore and Reynolds (1989). Step-scanned data were collected from 2° to 34° 2θ with a fixed rate of 2° per min with a step size of 0.05°2θ determined from oriented and glycolated clay slides. For the bulk minerals, the samples were prepared in the same manner described by Socorro and Maurrasse (2022), where the samples first were micronized for 10 min in a McCrone micronized mill with deionized water. After drying they were homogenized and packed into end-loading sample holders and then were analyzed on a Scintag XDS2000 diffractometer with data collection set from 2° to 60° 2 θ with a fixed time of 5 s per 0.05° 2θ for each sample. The mineral phases identified include quartz, potassium feldspar (K-feldspar), plagioclase feldspar (P-feldspar), calcite, dolomite, siderite, pyrite/marcasite, and bulk clay. All resulting traces were quantified using the semi-quantitative data reduction software from Materials Data Inc. (MDI) known as Jade+ and reported as relative percent.

3.5 Biomarker analysis

Twenty (20) samples targeting different lithologies were selected for biomarker analysis. The preparation for the biomarker analysis follows the procedures proposed by Socorro and Maurrasse (2019) and further explained in Herdocia and Maurrasse (2022). The total lipids were extracted by adding 5 g of powdered sample to a 10 mL solution of dichloromethane (DCM) and methanol (9:1) and sonicated for 30 min. The solution was then centrifuged, and the lipids were collected. This process was repeated twice for each sample. Elemental sulfur was removed by adding copper chippings to the extracts. Finally, the lipids were concentrated by evaporating the DCM and methanol, and the concentrate was left in 1 mL of *n*-hexane solution. The biomarker analysis was carried out at FIU's Advanced Mass Spectroscopy Facility using an Aligent 6,890 gas chromatography (GC) equipped with an HP-5MS UI capillary column (30 m, 0.250 mm, 0.25 μm). Detection was performed by an Aligent 5,973 single-quadrupole mass spectrometer (MS), using electron impact in positive mode. The MS was operated in Full Scan Mode between m/z 40 and 400. 5μL of each sample were injected into the GC with an injection temperature of 280 °C. The temperature program used for the biomarker analysis was as follows: hold at 65 °C for 2 min, increase to 300 °C at a rate of 4°C/min, and hold at 300 °C for 8 min.

As applied at previous sites in the Iberian Peninsula (Socorro et al., 2017; Socorro and Maurrasse, 2019) we also used normal alkane (*n*-alkane) chain lengths as a proxy to better characterize the relative proportion of land-derived in contrast with marine-derived OM. The ratio of terrestrial to aquatic extracts or TAR is calculated by dividing the sum of the longer odd-numbered *n*-alkanes by the sum of the shorter chain odd-numbered *n*-alkanes (Bourbonniere and Meyers, 1996; Peters et al., 2005; Holtvoeth et al., 2010).

$$TAR = nC_{27} + nC_{29} + nC_{31} / nC_{15} + nC_{17} + nC_{19}$$

Values below 1 indicate a predominance of marine derived OM, while values above 1 indicate a predominance of terrestrial OM.

The relative abundance of odd to even numbered carbons for the long chain *n*-alkanes ($\geq nC_{24}$) was used to determine the carbon preference index (CPI) (Bray and Evans, 1961):

$$CPI = \left[\frac{nC_{25} + nC_{27} + nC_{29} + nC_{31} + nC_{33}}{nC_{24} + nC_{26} + nC_{28} + nC_{30} + nC_{32}} + \frac{nC_{25} + nC_{27} + nC_{29} + nC_{31} + nC_{33}}{nC_{26} + nC_{28} + nC_{30} + nC_{32} + nC_{34}}\right] / 2$$

The odd-to-even predominance of the long chain *n*-alkanes ($>nC_{24}$) was determined using the OEP (2) after Peters et al. (2007) which was modified after Scalan and Smith's (1970) OEP equation as follows:

$$OEP\,(2) = (nC_{25} + 6nC_{27} + nC_{29}) / (4nC_{26} + 4nC_{28})$$

3.6 Pearson correlations

All correlation come from Microsoft Excel 2016, using Pearson's r equation (1896):

$$r = \frac{\sum (x_i - \bar{x})(y_i - \bar{y})}{\sqrt{\sum (x_i - \bar{x})^2 \sum (y_i - \bar{y})^2}}$$

In the formula, x_i and y_i are the corresponding sample values, and their corresponding sample averages are indicated by $\bar{x}$ and $\bar{y}$. All r-values are in the range of −1 to 1. A value of −1 is equivalent to a perfect negative correlation, 0 indicates that there is no correlation, and an r-value of 1 is equals a perfect correlation.

4 Results

4.1 Carbon geochemistry (TIC, TOC, and $\delta^{13}C_{org}$)

TIC, TOC, $\delta^{13}C_{org}$ were measured in all 83 samples; their values are plotted in Figure 3 (Table 1). TIC content for the 67.27 m studied section range from 0.1% to 86.0% (Figure 3B). TIC in the lower 6 m of the section fluctuates from 5.5% in the marlstone beds to 86.1% in the limestones and includes the Umbrera Formation (0–2.36 m) as well as the lowermost Patrocinio Fm. The overlying 38.7 m (SC-17-13 to SC-17-55; 7.04 m–44.72 m) is a part of the lower Patrocinio Formation which yielded TIC values between 3.4% and 25.4%. TIC in the upper Patrocinio Formation (44.72 m–67.27 m) is more

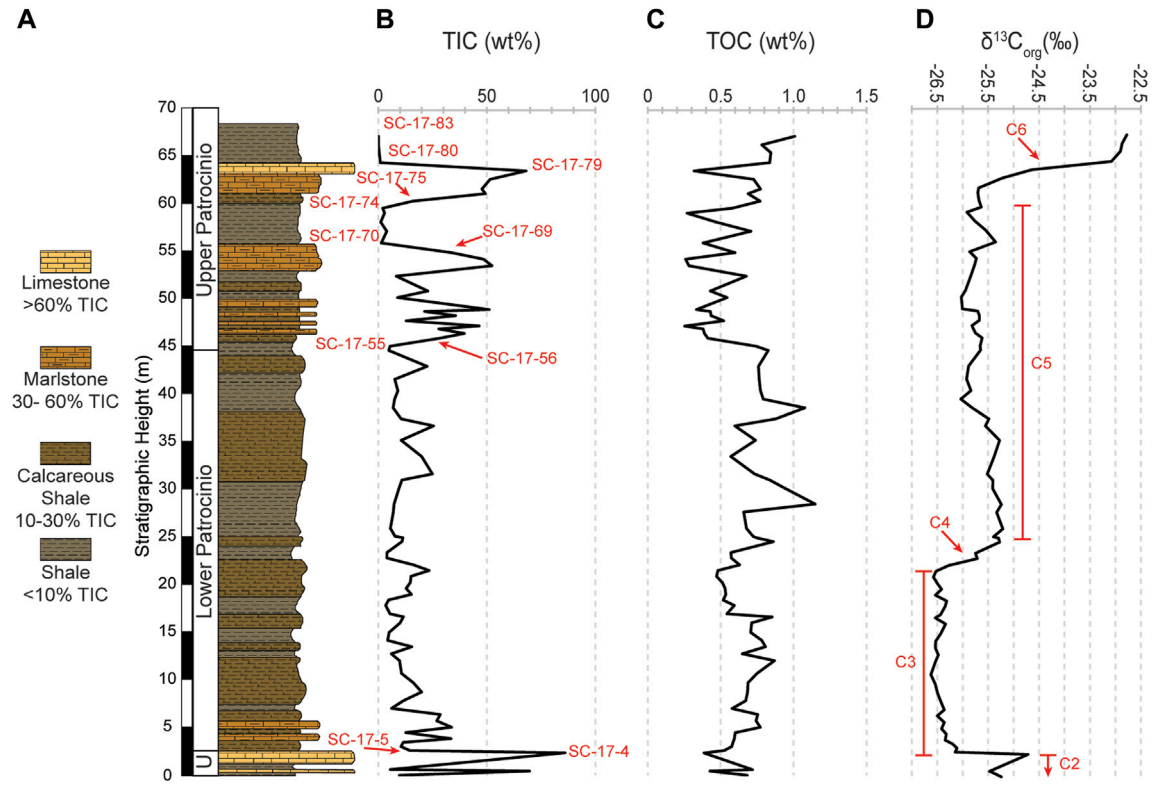

FIGURE 3
(A) Simplified stratigraphic column of the studied interval showing the variable lithologies. **(B)** Vertical distribution of the TIC. **(C)** Vertical distribution of the TOC. **(D)** Vertical distribution of the carbon isotope ($\delta^{13}C_{org}$) with the corresponding isotope segments after Menegatti et al. (1998).

variable with fluctuations from 68.1% down to 0.1%. A closer look in the Upper Patrocinio shows that above 44.72 m up to 55.02 m (SC-17-56 to SC-17-69), TIC values fluctuate between 8.3% and 52.4%. These high values are followed by a drop in TIC between 1.1% and 3.9% up to the height of 56.69 m (SC-17-70 to SC-17-74). Sequentially to 63.62 m (SC-17-75 to SC-17-79) TIC increases again from 15.9% up to 68.1%. The top of the studied section, above 56.69 m (SC-17-80 to SC-17-83) shows a significant drop in TIC values between 0.1% and 0.9%.

TOC values vary between 0.3% and 1.2%, with an average of 0.6% (Figure 3C). The lowest part of section (0–16.68 m; SC-17-1 to SC-17-24) shows increasing TOC values between 0.4% and 0.9%, whereas in the succeeding ~4.56 m (17 m–21.56 m; SC-17-25 to SC-17-32), TOC values drop to a low fluctuation pattern (0.5%–0.6%). The subsequent ~16.51 m (22.16 m–38.67 m; SC-17-33 to SC -17-49) includes more pronounced variations in TOC values, between 0.6% and 1.2% and contains two peaks in TOC, 1.2% and 1.1% at 28.56 m and 38.67 m, respectively. In the overlying ~5.58 m (39.59 m–45.17 m; SC-17-50 to SC-17-55) TOC values are relatively constant (0.7%–0.8%). The uppermost ~21.27 m of the studied section up to 67.27 m (SC-17-56 to SC-17-83) shows TOC variations with high frequencies, between 0.3% and 1.0% with an overall upward increasing trend.

As shown in Figure 3D, carbon isotopic values ($\delta^{13}C_{org}$) vary between −26.6‰ and −22.8‰, with an average of −25.8‰. The $\delta^{13}C_{org}$ values fluctuate from −25.2‰ (0 m) to a small positive value of −24.7‰ at 2.36 m (Umbrera Fm), which is followed by an abrupt negative shift to −26.2‰ at 2.61 m, at the base of the Patrocinio Fm. This negative inflection extends from 2.61 m to 21.6 m with an average of −26.4‰. The following isotopic values show an abrupt positive shift of 1‰ from −26.3‰ at 22.16 m to −25.3‰ at 24.61 m. This positive shift continues with a slow decline up to 61.23 m, where the value is −25.7‰. Another strong positive shift of 2.9‰ occurs from 61.23 m reaching up to −22.8‰ at 67.27 m.

4.2 Major, biolimiting, and redox sensitive trace elements

Results for the analysis of major elements and RSTEs are plotted in Figure 4 and Figure 5 (Table 2). Commonly elemental concentration for major, bioessential, and RSTEs are measured to assess terrigenous supplies, nutrient availability for productivity and the influence of reducing conditions during sedimentation.

The major elements fluctuate with lithology as the highest values coincide with the shales while the lowest correspond with the limestones, and they share a strong negative correlation with TIC (r = Al, −0.95; Si, −0.99; Ti, −0.97). Al concentrations range between 3.06 mg/g to 88.01 mg/g and average 56.86 mg/g (Figure 4C). Si ranges between 19.46 mg/g and 205.92 mg/g (Figure 4D) and correlates strongly with Al (r = 0.95). Ti concentrations correlate

TABLE 1 Carbon geochemistry (TIC, TOC, $\delta^{13}C_{org}$) values for the Cuchía section with their respective sample ID and stratigraphic height. TIC is expressed as $CaCO_3$ wt%, TOC in C wt%, and $\delta^{13}C_{org}$ in per mill (‰).

Sample ID	Height (m)	TIC (CaCO3 wt%)	TOC (C wt%)	$\delta^{13}C_{org}$ (‰ PDB)	Sample ID	Height (m)	TIC (CaCO3 wt%)	TOC (C wt%)	$\delta^{13}C_{org}$ (‰ PDB)
SC-17-83	67.27	0.13	1.01	−22.8	SC-17-41	28.56	7.22	1.15	−25.2
SC-17-82	66.36	0.07	0.78	−22.9	SC-17-40	27.72	6.92	0.66	−25.3
SC-17-81	65.55	0.42	0.84	−22.9	SC-17-39	26	5.56	0.68	−25.2
SC-17-80	64.49	0.94	0.84	−23.1	SC-17-38	25.17	7.66	0.72	−25.4
SC-17-79	63.62	68.14	0.32	−24.6	SC-17-37	25.01	11.29	0.74	−25.3
SC-17-78	62.74	51.56	0.73	−25.2	SC-17-36	24.61	10.98	0.86	−25.3
SC-17-77	61.72	47.71	0.77	−25.7	SC-17-35	23.45	3.99	0.57	−25.7
SC-17-76	61.23	49.34	0.69	−25.7	SC-17-34	22.88	3.95	0.57	−25.7
SC-17-75	60.44	15.85	0.77	−25.7	SC-17-33	22.16	16.26	0.63	−26.3
SC-17-74	59.69	2.01	0.58	−25.6	SC-17-32	21.56	23.40	0.48	−26.5
SC-17-73	59.18	2.88	0.27	−25.9	SC-17-31	20.95	15.11	0.47	−26.6
SC-17-72	58.24	1.08	0.47	−25.8	SC-17-30	20.29	14.71	0.51	−26.5
SC-17-71	57.27	3.88	0.71	−25.5	SC-17-29	19.67	12.81	0.53	−26.4
SC-17-70	56.04	1.38	0.38	−25.4	SC-17-28	19.05	15.23	0.53	−26.5
SC-17-69	55.02	33.66	0.60	−25.9	SC-17-27	18.45	4.77	0.52	−26.3
SC-17-68	54.32	48.47	0.26	−25.7	SC-17-26	17.88	3.37	0.59	−26.3
SC-17-67	53.64	52.41	0.28	−25.8	SC-17-25	17	5.42	0.54	−26.4
SC-17-66	52.54	8.27	0.68	−25.8	SC-17-24	16.68	11.57	0.85	−26.5
SC-17-65	50.98	22.79	0.43	−25.9	SC-17-23	16.04	10.07	0.71	−26.3
SC-17-64	50.28	8.85	0.54	−26.0	SC-17-22	15.04	4.98	0.71	−26.4
SC-17-63	49.02	51.15	0.33	−26.0	SC-17-21	14.21	4.32	0.78	−26.5
SC-17-62	48.82	21.30	0.43	−25.7	SC-17-20	13.53	15.41	0.81	−26.5
SC-17-61	48.38	35.65	0.43	−25.7	SC-17-19	12.79	5.97	0.65	−26.5
SC-17-60	47.84	12.82	0.52	−25.7	SC-17-18	12.07	9.82	0.87	−26.5
SC-17-59	47.29	46.47	0.25	−25.8	SC-17-17	10.72	10.75	0.75	−26.6
SC-17-58	46.99	27.85	0.38	−25.8	SC-17-16	9.74	16.16	0.69	−26.5
SC-17-57	46.51	39.69	0.39	−25.7	SC-17-15	8.77	20.00	0.68	−26.5
SC-17-56	46	28.21	0.41	−25.6	SC-17-14	7.85	11.59	0.67	−26.4
SC-17-55	45.17	5.42	0.74	−25.7	SC-17-13	7.04	6.06	0.58	−26.4
SC-17-54	44.72	4.80	0.83	−25.6	SC-17-12	6.41	28.57	0.75	−26.5
SC-17-53	43.05	22.47	0.76	−25.9	SC-17-11	5.73	26.92	0.74	−26.4
SC-17-52	41.68	7.59	0.76	−25.9	SC-17-10	5.06	33.79	0.77	−26.4
SC-17-51	40.47	9.03	0.77	−25.8	SC-17-9	4.49	12.63	0.60	−26.3
SC-17-50	39.59	7.54	0.79	−26.0	SC-17-8	3.85	33.55	0.59	−26.3
SC-17-49	38.67	6.82	1.08	−25.8	SC-17-7	3.47	11.50	0.58	−26.2
SC-17-48	37.52	10.58	0.88	−25.5	SC-17-6	3.02	10.47	0.58	−26.1
SC-17-47	36.79	25.43	0.60	−25.6	SC-17-5	2.61	14.52	0.53	−26.1

(Continued on following page)

TABLE 1 (*Continued*) Carbon geochemistry (TIC, TOC, $\delta^{13}C_{org}$) values for the Cuchía section with their respective sample ID and stratigraphic height. TIC is expressed as $CaCO_3$ wt%, TOC in C wt%, and $\delta^{13}C_{org}$ in per mill (‰).

Sample ID	Height (m)	TIC (CaCO3 wt%)	TOC (C wt%)	$\delta^{13}C_{org}$ (‰ PDB)	Sample ID	Height (m)	TIC (CaCO3 wt%)	TOC (C wt%)	$\delta^{13}C_{org}$ (‰ PDB)
SC-17-46	35.28	10.56	0.74	−25.3	SC-17-4	2.36	86.04	0.39	−24.7
SC-17-45	33.57	19.97	0.57	−25.4	SC-17-3	0.6	5.45	0.72	−25.5
SC-17-44	31.73	24.90	0.73	−25.5	SC-17-2	0.44	69.72	0.43	−25.4
SC-17-43	31.09	10.86	0.84	−25.4	SC-17-1	0	9.67	0.68	−25.2
SC-17-42	30.22	9.52	0.94	−25.4					

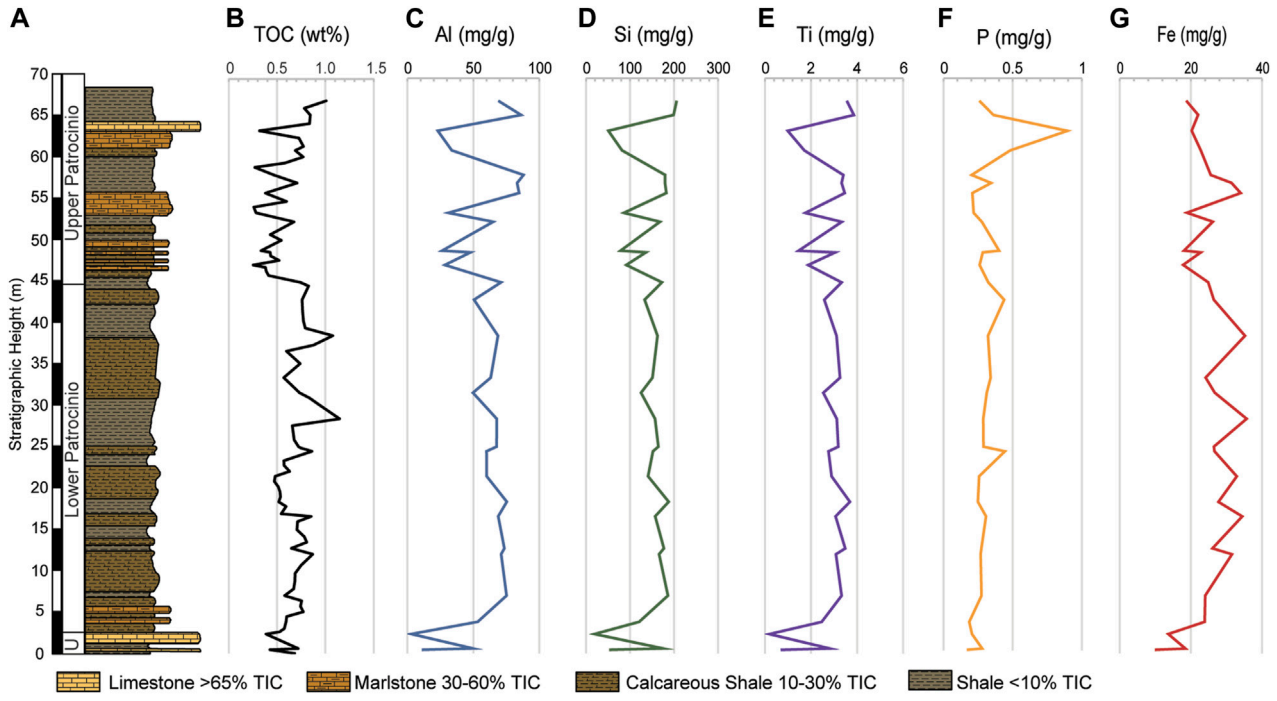

FIGURE 4
(A) Simplified stratigraphic column of the studied interval showing the variable lithologies. **(B)** Vertical distribution of the TOC. Vertical distribution of the major elements: **(C)** Aluminum, **(D)** Silicon, and **(E)** Titanium. Vertical distribution of the biolimiting elements: **(F)** Iron and **(G)** Phosphorus. Elemental values are displayed in mg/g.

strongly with Al (r = 0.96) and fluctuate between 0.20 mg/g and 3.86 mg/g (Figure 4E). These terrestrially derived elements show a positive correlation with TOC (r = Al, 0.51; Si, 0.56; Ti, 0.52) as shown in Figure 4.

Of the biolimiting elements (Fe, P), Iron follows a pattern like Al (r = 0.71) and shows a positive correlation with TOC (r = 0.52) (Figure 4G). In general, Fe is higher in the shales and decreases in the limestone, as indicated by its negative correlation with TIC (r = −0.65). By contrast, phosphorus has no apparent correlation with either Al (r = −0.21) or TOC (r = −0.01) and ranges from 0.17 to 0.89 mg/g with an average of 0.32 mg/g (Figure 4F).

The temporal distribution of the RSTEs (V, Cr, Ni, Mo, and U) is shown in Figure 5. Vanadium, and U show trends compatible with Al (V, r = 0.94 and U, r = 0.76) and of the measured RSTEs they share the strongest correlation with TOC (V, r = 0.50 and U, r = 0.51). Molybdenum behaves independently of the lithology, TOC, and the major elements.

4.3 Clay and bulk mineralogy

Figure 6 shows the results for the mineralogical analysis carried out for 9 samples at stratigraphic heights: 5.06 m (SC-17-10), 7.04 m (SC-17-13), 14.21 m (SC-17-21), 28.56 m (SC-17-41), 36.79 m (SC-17-47), 47.84 m (SC-17-60), 57.27 m (SC-17-71), 61.23 m (SC-17-76), and 66.36 m (SC-17-82). The bulk of the clay mineralogy is composed of Illite (64.9%–78.6%; Figure 6B). Smectite and illite contents seem to drop at stratigraphic heights with high TOC but

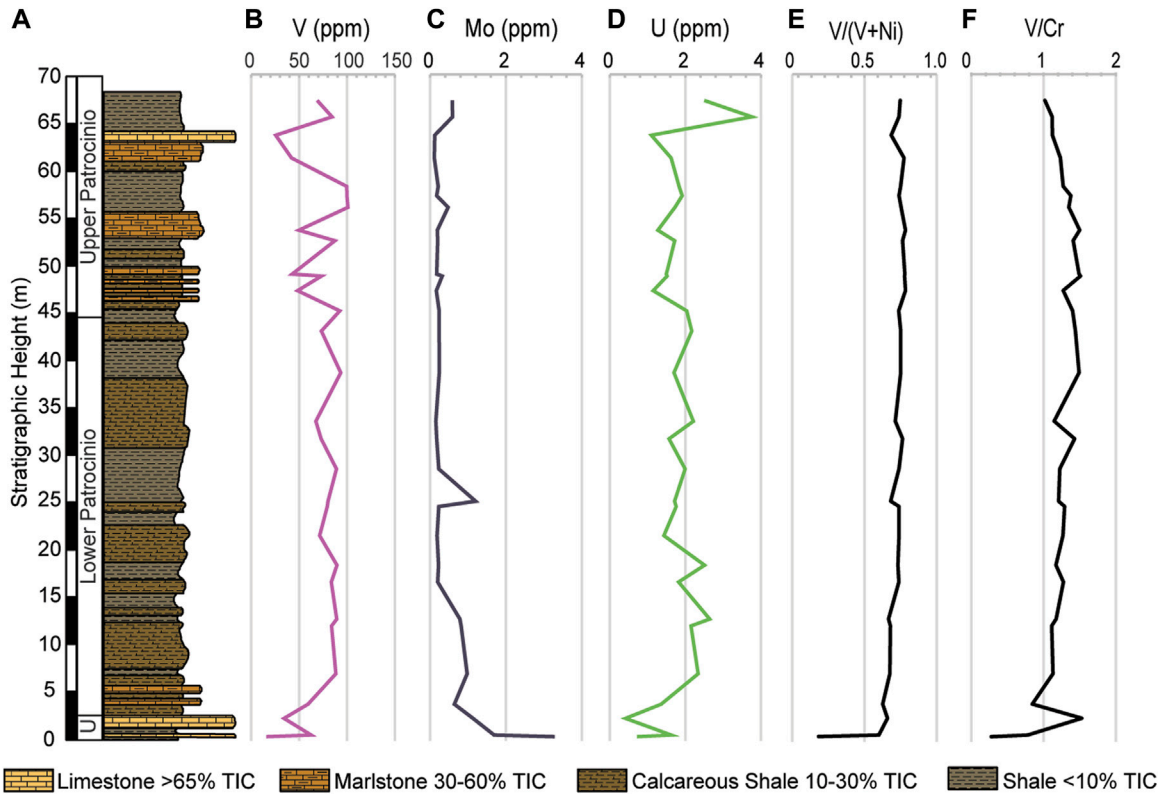

FIGURE 5
(A) Simplified stratigraphic column of the studied interval showing the variable lithologies. Vertical distribution of the RSTEs **(B)** Vanadium, **(C)** Molybdenum, **(D)** Uranium, **(E)** V/(V+Ni), and **(F)** V/Cr. Values are displayed in part per million (ppm).

increase where TIC is high, whereas Kaolinite and chlorite percentages decrease where TIC is higher. Chlorite shows minor variations between 6.9% and 10.9%. Kaolinite content fluctuates from 11.3% to 21.5%. Smectite is in the lowest abundance of the clays (0.8%–3.8%). Figure 6C shows the bulk mineralogical abundances averaged for the 9 analyzed samples. The most abundance mineral is quartz (42%) followed by clay minerals (17%) then siderite (14%), calcite (10%), P-feldspar (6%), K-feldspar (5%), dolomite (4%), and pyrite/marcasite (2%).

4.4 Biomarkers

The twenty samples analyzed for *n*-alkanes and the acyclic isoprenoids pristane (Pr) and phytane (Ph) (Figure 7). Twelve (12) samples at the respective heights of 0.6 m, 3.85 m, 7.04 m, 12.07 m, 15.04 m, 19.05 m, 24.61 m, 38.67 m, 50.28 m, 53.64 m, 57.28 m, and 67.27 m (Figure 7C), have a bimodal distribution with one peak centered at nC_{15} and the other between nC_{25} and $nC_{28,}$ (Figures 7D,G–I). The remaining 8 samples (heights: 28.56 m, 33.57 m, 43.05 m, 46.0 m, 47.84 m, 49.02 m, 61.23 m, and 63.62 m) display a right skewed (positive) unimodal distribution (Figures 7E,F). The chromatograms for four representative examples (Figure 8) reveal mostly low unresolved complex mixture (UCM) for the aliphatic fraction. The TAR values throughout the section range from 0.06 up to 1.41 with an average of 0.43 (Table 3; Figure 7C). In the lower part TAR values vary from 0.48 up to 1.41 at stratigraphic height 19.05 m, which corresponds to the highest values attained. The TAR values decrease from 1.41 to 0.15 at 25.56 m and remain below 0.5 until 63.62 m. Generally, the *n*-alkane distribution has an inverse relationship with TIC (r = −0.46) as higher TIC coincides with lower TAR values, whereas low TIC corresponds with higher TAR values.

The *n*-alkanes with chain lengths greater than nC_{24} have an average CPI of 0.82 (from 0.6 to 1.4) and an average OEP (2) of 0.75 (from 0.5 to 1.5) indicating that the succession has mostly an even carbon number preference (Table 3). Pristane and Phytane ratios (Pr/Ph) are listed on table 3 and range from 1.4 to 5.0 with an average of 2.19. Values for Pr/nC_{17} and Ph/nC_{18} are low, averaging 0.31 and 0.23, respectively.

5 Discussion

5.1 Chemostratigraphic correlation

Temporal CIEs ($\delta^{13}C_{org}$ and $\delta^{13}C_{carb}$) coeval with OM-rich intervals recorded in Aptian sediments worldwide are widely accepted to represent global disruptions in the carbon cycle (e.g., Scholle and Arthur, 1980; Arthur et al., 1985; Jenkyns, 1995; Kuhnt et al., 1998; Menegatti et al., 1998; Leckie et al., 2002; de Gea et al.,

TABLE 2 Absolute values of the terrestrially derived elements (Al, Si, and Ti), biolimiting elements (Fe and P), and redox sensitive trace elements (RSTEs) (V, Ni, Co, Cr, Cu, and Mo) of the Cuchía section. Concentrations for major and biolimiting elements are reported in mg/g and the RSTEs as parts per million (ppm).

Sample ID	Height (m)	Al (mg/g)	Si (mg/g)	Ti (mg/g)	P (mg/g)	Fe (mg/g)	V (ppm)	Cr (ppm)	Ni (ppm)	Mo (ppm)	U (ppm)	V/(V+Ni)	V/Cr
SC-17-83	67.27	68.96	205.92	3.55	0.26	18.69	68.8	67.7	23.1	0.58	2.50	0.75	1.02
SC-17-81	65.55	86.22	199.02	3.86	0.36	22.02	84.3	75.3	29.6	0.59	3.76	0.74	1.12
SC-17-79	63.62	23.00	50.72	0.99	0.89	20.21	25.5	22.7	11.7	0.12	1.10	0.69	1.12
SC-17-76	61.23	33.66	81.81	1.71	0.48	22.77	42.1	34.1	12.2	0.11	1.62	0.78	1.23
SC-17-72	58.24	88.01	179.84	3.40	0.21	25.58	99.7	78.2	32.9	0.21	1.83	0.75	1.27
SC-17-71	57.27	83.20	179.60	3.33	0.35	31.38	99.9	72.4	35.0	0.17	1.92	0.74	1.38
SC-17-70	56.04	84.67	182.58	3.46	0.21	33.98	100.9	74.7	32.6	0.47	1.72	0.76	1.35
SC-17-67	53.64	31.13	86.12	1.75	0.22	18.88	49.7	33.1	13.6	0.19	1.27	0.79	1.50
SC-17-66	52.54	65.01	168.04	3.33	0.28	26.13	87.3	61.8	26.7	0.20	1.72	0.77	1.41
SC-17-63	49.02	26.28	78.44	1.46	0.40	18.06	42.6	28.5	12.0	0.17	1.50	0.78	1.49
SC-17-62	48.82	47.89	136.26	3.05	0.29	22.77	73.3	48.4	20.7	0.32	1.52	0.78	1.51
SC-17-59	47.29	28.40	91.41	1.87	0.26	17.83	48.3	38.0	13.2	0.16	1.15	0.79	1.27
SC-17-55	45.17	70.98	172.59	3.33	0.33	24.86	92.4	65.8	32.6	0.24	2.03	0.74	1.40
SC-17-53	43.05	50.47	133.17	2.57	0.44	26.43	73.1	50.7	24.1	0.24	2.17	0.75	1.44
SC-17-49	38.67	68.71	162.36	3.10	0.32	35.19	93.4	62.5	30.7	0.24	1.70	0.75	1.49
SC-17-45	33.57	63.20	151.09	3.26	0.34	24.14	67.4	58.7	26.9	0.15	2.21	0.71	1.15
SC-17-44	31.73	49.71	125.03	2.53	0.31	26.70	73.0	50.9	22.3	0.17	1.57	0.77	1.43
SC-17-41	28.56	67.71	157.00	3.12	0.29	35.65	88.9	72.6	31.1	0.23	1.99	0.74	1.23
SC-17-38	25.17	67.63	164.50	3.18	0.29	26.46	80.2	66.3	37.4	1.20	1.71	0.68	1.21
SC-17-36	24.61	60.01	152.27	2.76	0.44	26.60	79.3	61.3	27.8	0.23	1.76	0.74	1.29
SC-17-32	21.56	60.07	140.93	2.89	0.26	32.88	71.4	56.2	25.0	0.18	1.43	0.74	1.27
SC-17-27	18.45	75.40	187.80	3.69	0.25	27.74	89.5	76.3	32.6	0.22	2.51	0.73	1.17
SC-17-24	16.68	68.83	157.29	3.06	0.31	34.41	83.5	65.4	29.4	0.20	1.82	0.74	1.28
SC-17-19	12.79	73.56	177.09	3.48	0.28	26.07	89.2	75.9	44.4	0.78	2.64	0.67	1.18
SC-17-18	12.07	71.06	166.08	3.08	0.27	31.52	83.9	75.3	39.3	0.82	2.15	0.68	1.11
SC-17-13	7.04	75.23	186.08	3.33	0.28	24.01	88.3	78.1	42.1	0.98	2.34	0.68	1.13
SC-17-8	3.85	53.26	120.85	2.46	0.19	23.88	59.3	70.3	35.3	0.64	1.36	0.63	0.84
SC-17-4	2.36	3.06	19.46	0.20	0.21	13.64	34.3	22.4	17.6	1.13	0.42	0.66	1.53
SC-17-3	0.6	49.55	174.87	2.81	0.28	18.45	62.5	80.1	41.7	1.69	1.63	0.60	0.78
SC-17-2	0.44	10.91	52.75	0.69	0.17	9.86	15.8	58.1	71.7	3.28	0.72	0.18	0.27

2003; Godet et al., 2006; Michalík et al., 2008; Tejada et al., 2009; Sanchez-Hernandez and Maurrasse, 2016; Hu et al., 2020; Socorro and Maurrasse, 2022). Potential local variations in the amplitude of the carbon isotope curve have also been examined because of modulating factors such as terrestrial OM and species–specific fractionation (Ravelo and Fairbanks, 1995; Taylor et al., 2001; Anderson et al., 2005), OM source and biochemical pathways (e.g., Pardue et al., 1976; Cranwell, 1981; Ponton et al., 2014; Feakins et al., 2007; Feakins et al., 2016; Basu et al., 2015) as well as diagenesis. While these previous factors may affect the Cuchía site, another factor related to tectonic controls on the long-term carbon isotope mass balance (Shields and Mills, 2017) can be ruled out, because covariations of the defined carbon isotopic segment associated with OM-rich sediments of the studied section have been satisfactorily used on a wide geographic scale (Millán et al., 2009; Moosavizadeh et al., 2014; Sanchez-Hernandez and Maurrasse, 2014; Sanchez-Hernandez and Maurrasse, 2016; Socorro and Maurrasse, 2019). Since the isotopic segments have also been

well-tested and calibrated to magnetostratigraphy and biostratigraphy (Channell and Erba, 1992; Channell et al., 2000; Herrle et al., 2004; Godet et al., 2006), the effectiveness of the $\delta^{13}C_{org}$ and the $\delta^{13}C_{carb}$ curve can be considered a robust and useful tool for cross correlation between sites. Thus, despite the modulating factor from terrestrial sources the carbon isotopic curve is a reliable chronostratigraphic proxy for the Aptian stage. Based on this premise, we use these segments to contrast the studied site with other well-studied sections, namely, the El Pui section (Sanchez-Hernandez and Maurrasse, 2016), the Cismon section, and the Roter Sattel section (Menegatti et al., 1998) to confirm the Cuchía timeline in the global context (Figure 10).

The $\delta^{13}C_{org}$ values at the base of the studied section fluctuate from −25.2‰ (0 m) to a value of −24.7‰ at 2.36 m at the top of the Umbrera Fm which can be assigned to the uppermost part of C2 (Figure 10D). This spike is followed by an abrupt negative shift to −26.2‰ at 2.61 m and reaches the most negative value of ~-26.5‰ at 21.56 m. A similar pattern is observed at Roter Sattel (Switzerland), toward the end of C2 (~3.5 m) with a C-isotope value of ~-27.2‰, then at 4 m it reaches a peak of −26.4‰, marking the end of segment C2, which is followed by a negative excursion to a low of −28.8‰ indicative of the end of C3. In the Cismon section (Italy), segment C2 ends with a maximum of ~-24.0‰ which is succeeded by fluctuating values that end with a sharp negative value of ~-28.4‰ marking the close of C3 (Menegatti et al., 1998). By comparison, in the El Pui section (Catalunya, Spain), segment C2 ends with a maximum of −25.0‰ at 163 m, followed by a sharp decline to ~-27.2‰ corresponding with the start of the negative trend characteristic of C3 which reaches its lowest value of ~-28.0‰ at 199 m (Sanchez-Hernandez and Maurrasse, 2016).

The remarkable distinction of the C3 negative trend recorded in the lower part of the Patrocinio Fm (2.61m - 21.56 m) is the low amplitude fluctuation of the $\delta^{13}C_{org}$ values from ~-26.6‰ to ~-26.1‰, a shift of only ~-1.8‰. By comparison, the three coeval sites yield the following changes: Roter Sattel ~-2.4‰; Cismon ~-4.4‰; El Pui ~-3.0‰ (Figures 10A–C). As we will discuss further the cause of this discrepancy, sediments of the NBCB at the Cuchía site recorded the least negative values of this distinct CIE that is the hallmark of the C-isotope curve marking the onset of OAE1a.

A similar divergence is recorded in the Cuchía section for the conventional negative CIE assigned to C4 which is marked by a 1‰ positive shift from −26.3‰ at 22.16 m to −25.3‰ at 24.61 m. By contrast, in the Roter Sattel section segment C4 (Figure 2 in Menegatti et al., 1998) is defined by ~3.4‰ positive inflection from −28.8‰ to about −25.4‰. Similarly, in the Cismon section (Figure 3 in Menegatti et al., 1998) segment C4 is represented by a ~2.5‰ positive shift from ~−28.4‰ to ~−25.9‰, whereas in the El Pui section segment C4 is characterized by ~3.7% positive shift extending ~13 m, (199 m–~212 m) with an isotope value ranging from −27.9‰ to −24.2‰ at 212 m (Sanchez-Hernandez and Maurrasse, 2016).

The succeeding $\delta^{13}C_{org}$ values assigned to segment C5 in the Cuchía section start with ~-25.3‰ at the end of segment C4 and remain steady around −25.7‰ ending with a value of ~-25.7‰ at 61.72 m (Figure 10D). By comparison, segment C5 in the Roter Sattel section yields isotope values between −25.6‰ and −24.8‰ with little variation (~0.8‰), whereas in the Cismon section isotope values for segment C5 fluctuate between ~−26.0‰ and −23.6‰ (~2.4‰) with no sudden increase or decrease within the segment. In the conjoint El Pui - El Pujal section (Sanchez-Hernandez and Maurrasse, 2016; Socorro and Maurrasse, 2019; Socorro and Maurrasse, 2022) segment C5 varies between −25.3‰ and ~-22.6‰, with an amplitude of ~2.7‰. The final 5.5 m portion of the studied Cuchía section may be attributed to carbon-isotope segment C6 because it shows another strong 2.9‰ positive shift with values from −25.7‰ up to −22.8‰ at 67.27 m (Figure 10D). Likewise, in the Roter Sattel section a sharp positive CIE of ~2.0‰ defines carbon-isotope segment C6 with an increase from about ~-25.6‰ to ~-23.6‰ (Figure 10A). A comparable abrupt fluctuation is also recorded in the Cismon section which shows a ~3.2‰ increase from −25.2‰ to ~-22.0‰ (Figure 10B).

In essence, the pattern of $\delta^{13}C_{org}$ fluctuation in the studied Cuchía section correlated to Roter Sattel, Cismon and El Pui permits to identify segments C2 to C6 (Figure 10) coinciding with previous studies (Najarro et al., 2011a; Najarro et al., 2011b). Carbon isotope values at the Cuchía site vary from −26.6‰ to −22.8‰, giving a spread of 3.8‰, thus revealing that the most negative values occur within segment C3, identical to the record in the other correlative sections. Non-etheless, the values are less negative in the NBCB compared to elsewhere (Figure 10). The main difference is the overall amplitude of the isotopic values in C3 that is more positive at Cuchía. The Cismon, Roter Sattel, and the El Pui sections share very similar values, the lowest value in all three sites is about −28‰ within segment C3 and their maximum values in C6 are around −22‰, giving all three sites about a six ‰ spread, or nearly 40% larger. In the following section we further discuss the possible factors that may have caused the differences between the range of $\delta^{13}C_{org}$ values in Cuchía and the correlative sites.

5.2 Assessing the degree of thermal maturity and reliability of the biomarkers

The true OM signal may be affected by thermal alteration that brings bias to the data; therefore, the degree of thermal maturity is an important parameter to assess the reliability of the OM present. Commonly, bimodal distributions in the *n*-alkanes are lost with increasing degree of thermal maturity because hydrocarbons are selectively removed (Peters et al., 2005). Given that 12 out of 20 of the chromatograms for the biomarkers (Figure 7C) have a bimodal distribution, therefore the degree of thermal degradation is likely moderate in the studied section.

The degree of thermal degradation may be further tested by calculating the relative abundance of odd to even numbered carbons in the long chain *n*-alkanes using the CPI and OEP (2) (Peters et al., 2005). In general, as CPI and OEP (2) values approaches ~1 thermally maturity increases, while values significantly above 1.0 are indicative of an odd preference, and values significantly below 1.0 point to an even carbon preference (Bray and Evans., 1961; Peters et al., 2005). The long chain *n*-alkanes show a CPI that ranges from 0.61 to 1.55 with an average of 0.89, and OEP (2) values from 0.47 to 1.47 with an average of 0.75 (Table 3). Both ratios suggest that the samples

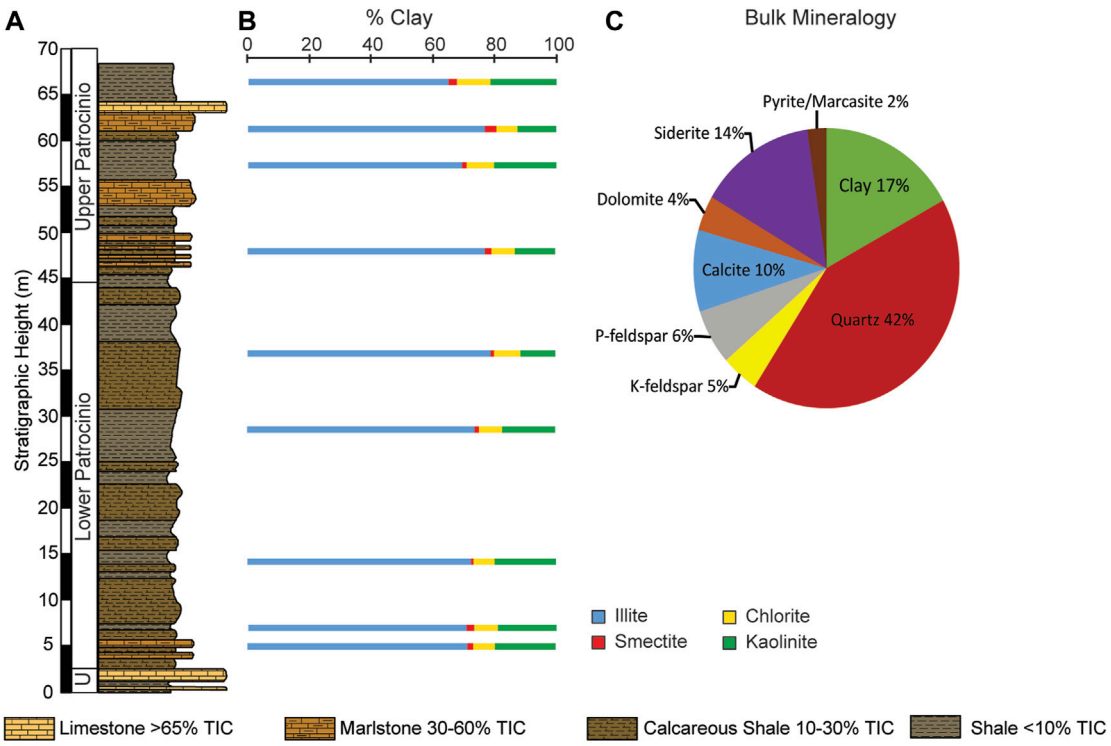

FIGURE 6
(A) Simplified stratigraphic column of the studied interval showing the variable lithologies. **(B)** Vertical distribution of the relative abundances of the clay minerals: illite, smectite, chlorite, and kaolinite for 9 samples at stratigraphic heights: 5.06 m (SC-17-10), 7.04 m (SC-17-13), 14.21 m (SC-17-21), 28.56 m (SC-17-41), 36.79 m (SC-17-47), 47.84 m (SC-17-60), 57.27 m (SC-17-71), 61.23 m (SC-17-76), and 66.36 m (SC-17-82). **(C)** Average bulk mineralogical abundances of the nine samples analyzed for clay mineralogy.

have an even carbon number preference and corroborates some degree of thermal alteration as the values are close to 1.0. Usually, OM derived from terrigenous sources display a predominance of odd-over-even carbon number of long chain *n*-alkanes ($\geq nC_{25}$), which is disclosed particularly for nC_{27}, nC_{29}, and nC_{31}, but this preference may disappear during early diagenetic processes (Johnson and Calder, 1973; Nishimura and Baker, 1986; Kuhnt et al., 1998; Peters et al., 2005). In the Cuchía section most of the long chain *n*-alkanes show an even-over-odd preference, except at a height of 12.07 m and 67.27 m. The lack of odd-over-even carbon preferences throughout the section points to low to moderate degree of diagenetic alteration that may not significantly alter their original characteristics.

By comparison, biomarkers from three other sites elsewhere within the Basque-Cantabrian Basin, southeast and east of Cuchía (Quijano et al., 2012), similarly showed that C_{22}-C_{30} *n*-alkanes had an even carbon number preference (OEP = 0.69—0.80; Chaler et al., 2005). This even carbon preference was attributed to strong reducing conditions which can favor the formation of even-carbon-number from fatty acids and waxy alcohols. Yet, as discussed above, RSTEs in the Cuchía section correlate strongly with the major elements, thus indicating that this part of the basin may not have experienced strong reducing conditions. The mechanism proposed by Chaler et al. (2005) probably played a role in the even carbon preference at Cuchía but was also modulated by thermal alteration.

In other parts of the NBCB, previous biomarker results based on hopane and sterane ratios at the Puentenansa section (named La Florida section in Najarro et al., 2011b) to the southwest of the Cuchía section (Figure 1A), at a level equivalent to the Patrocinio Fm, contained thermally mature OM within the peak oil generation window (Quijano et al., 2012). Given that the NBCB experienced uneven subsidence rates (Najarro et al., 2011b) it can be inferred that different parts of the NBCB experienced dissimilar thermal histories since basin subsidence leads to increased depth of burial and thus higher geothermal effects (Feinstein, 1981). In fact, as shown by Najarro et al. (2011a), Najarro et al. (2011b) the Puentenansa section experienced slightly higher subsidence rates than the Cuchía area. Thus, based on the bimodal distribution, the CPI and the OEP (2) values, we can surmise that the rocks in the Cuchía section are probably either within the oil window, or perhaps in the early oil window and support the accuracy of the isotopic data.

5.3 Significance of the biomarkers indicative of provenance

To elucidate the intricate paleoenvironmental evolution of the NBCB recorded in the Cuchía section it is important to consider the

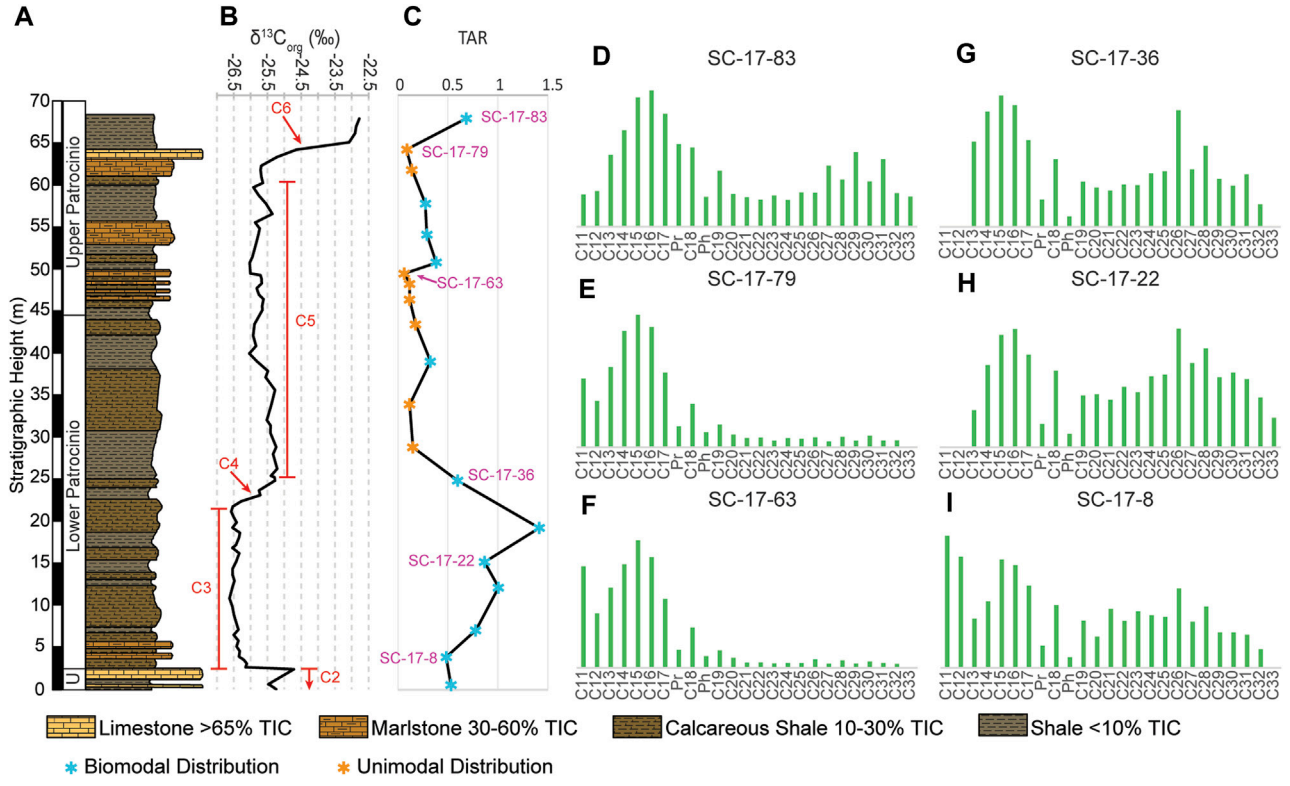

FIGURE 7
(A) Simplified stratigraphic column of the studied interval showing the variable lithologies. **(B)** Vertical distribution of the carbon isotope ($\delta^{13}C_{org}$) with the corresponding isotope segments after Menegatti et al. (1998) for comparison with biomarker proxies. **(C)** Vertical distribution of the terrestrial aquatic ratio (TAR) with stars to indicate bimodal distribution (blue stars) and unimodal distributions (orange stars) in the *n*-alkanes. **(D–I)** 6 representative *n*-alkane distribution patterns taken from 3.85 m, 15.04 m, 24.61 m, 24.61 m, 63.62 m, and 67.27 m.

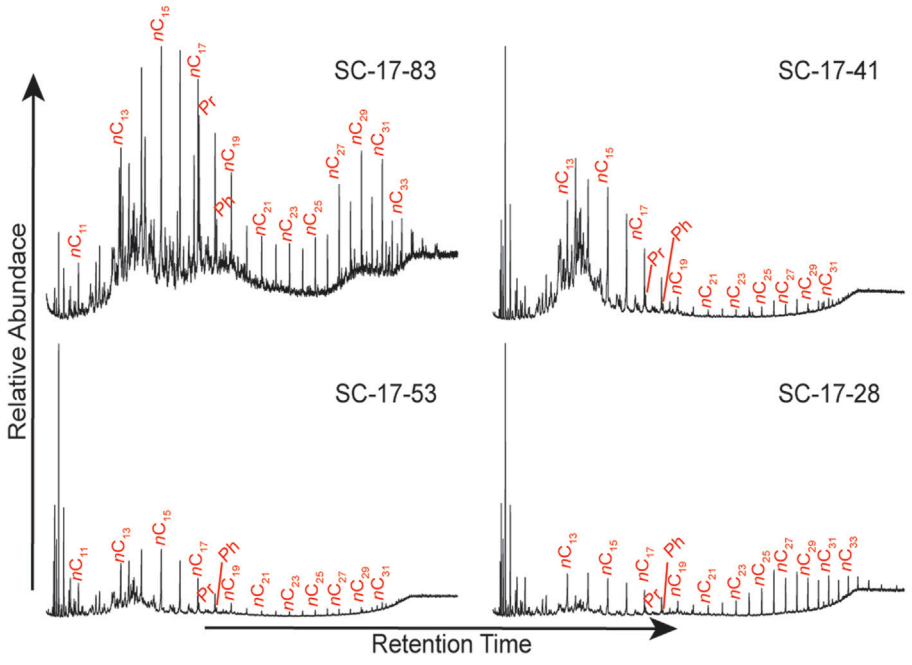

FIGURE 8
Chromatograms of selected samples along the studied section.

TABLE 3 List of biomarker ratios with their corresponding sample number and stratigraphic position: terrestrial aquatic ratio (TAR), pristane and phytane ratios (Pr/Ph), carbon preference index (CPI), and the odd-to-even predominance OEP (2).

Sample ID	Height (m)	TAR	Pr/Ph	CPI	OEP (2)
SC-17-83	67.27	0.68	2.75	1.55	1.47
SC-17-79	63.62	0.08	1.39	0.65	0.62
SC-17-76	61.23	0.14	2.24	0.61	0.63
SC-17-71	57.28	0.27	1.78	0.63	0.61
SC-17-67	53.64	0.29	2.48	0.90	0.89
SC-17-64	50.28	0.38	1.61	0.98	0.81
SC-17-63	49.02	0.06	1.51	0.63	0.53
SC-17-60	47.84	0.12	2.93	0.77	0.66
SC-17-56	46	0.12	1.49	0.65	0.47
SC-17-53	43.05	0.18	2.71	1.33	0.96
SC-17-49	38.67	0.33	2.94	0.68	0.62
SC-17-45	33.57	0.12	1.55	0.86	0.66
SC-17-41	28.56	0.15	1.65	0.82	0.69
SC-17-36	24.61	0.60	2.63	0.75	0.57
SC-17-28	19.05	1.41	5.00	1.00	0.80
SC-17-22	15.04	0.87	1.72	0.87	0.75
SC-17-18	12.07	1.01	1.43	1.44	1.13
SC-17-13	7.04	0.78	2.20	0.93	0.74
SC-17-8	3.85	0.48	2.07	0.76	0.64
SC-17-3	0.6	0.53	1.79	1.04	0.78

possible modulating effects of paralic influences as suggested in previous studies (Najarro et al., 2011b). We use *n*-alkanes as a proxy to characterize the type of OM preserved and determine the temporal contribution of the land derived components to the basin. The chain length of the *n*-alkanes are well recognized proxies that can be used to determine the source of the OM because short chain *n*-alkanes ($\leq nC_{19}$) are mainly derived from marine plankton and/or microbial communities (Cranwell, 1973; Cranwell et al., 1987; Forster et al., 2004; Peters et al., 2005), whereas chain lengths between nC_{20} to nC_{25} tend to be produced by marine and non-marine aquatic macrophytes (Ficken et al., 2000), and terrestrial plants produce longer chain *n*-alkanes ($\geq nC_{25}$) (Peters et al., 2005).

The chronological distribution of the biomarker data from the Cuchía section revealed a range of *n*-alkanes from nC_{11} to nC_{33} (Figure 7), thus implying a mixed OM content throughout the length of the studied interval. Of the 20 samples analyzed, 8 have a unimodal distribution centering on nC_{15} indicative of a predominance of OM derived from marine organisms. Twelve (12) samples have a bimodal distribution with one peak centered at nC_{15} and the second peak centered between nC_{25} and nC_{28} (Figure 7C). In all cases, the short-chain *n*-alkanes are most abundant, therefore they are indicative of a predominance of OM mostly derived from microbial phytoplankton and aquatic macrophytes, although the long-chain *n*-alkanes also disclose significant contribution of terrestrial plants (Dañobeitia et al., 1990; Frakes et al., 1992; Kuhnt et al., 1998; de Gea et al., 2003; Forster et al., 2004). This mix composition is corroborated by the Pr/nC_{17} and Ph/nC_{18} plot (Figure 9) which shows that the OM is mostly within marine type II kerogen, as well as mixed type II/III kerogen emblematic of both marine and terrestrial contribution (Peters et al., 2005). Sample SC17-28 (19.05 m) is the only one that plots in terrigenous type III kerogen. Nevertheless, uncertainty may arise in the interpretation because these ratios can be affected through biodegradation since bacteria preferentially degrade hydrocarbons. Typically, the *n*-alkanes will be removed first, especially the low molecular weight *n*-alkanes, followed by the acyclic isoprenoids (Pr and Ph) (Peters et al., 2005). The extent of such changes can be easily identified in the chromatograms by the UCM which becomes increasingly more prominent as these compounds are removed. The samples at Cuchía have very low UCM humps at all analyzed levels as well as higher proportions of *n*-alkanes to the acyclic isoprenoids (Figure 8), therefore they were preserved with minimal biodegradation.

Further assessment of the provenance relative to the contribution of terrigenous *versus* marine OM can be more distinctly discerned using the TAR (Figure 7C) which compares the relative abundances of short chain *n*-alkanes (nC_{15}, nC_{17}, nC_{19}) derived from marine OM (Cranwell, 1973; Cranwell et al., 1987; Socorro and Maurrasse, 2019; Socorro and Maurrasse, 2020), to the long chain *n*-alkanes (nC_{27}, nC_{29}, nC_{31}) produced by terrestrial plants (Peters et al., 2005). Higher TAR values correspond to increased terrigenous OM (Bourbonniere and Meyers, 1996). In the Cuchía samples TAR generally follows lithology (TAR vs. TIC, r = −0.46), thus indicating heightened terrigenous OM input at levels with decreased carbonate content. Additionally, the TAR temporal variation follows a trend comparable to the Al content (r = 0.53), revealing that terrestrial pulses are the main delivery method for the terrestrial biomarkers (Hedges et al., 1997). The highest TAR values tend to correspond primarily with the lowermost part of the sequence (below 24.61 m) with a ratio up to 1.41. Although the average TAR value of 0.43 reveals that the OM was predominantly produced by marine microbial phytoplankton, long chain *n*-alkanes ($\geq nC_{25}$) are found at all measured levels, which corroborates sustained input from terrigenous sources, especially below 24.61 m where TAR values are highest. This data agrees with the Pr/nC_{17} and Ph/nC_{18} plot (Figure 9) as well as the gymnosperm pollens revealed in a previous study (Najarro et al., 2011b).

5.4 Assessing the cause of varying carbon-isotope values in the correlative sections

In the Cuchía sediments the C-isotopic values correlated with the sections elsewhere are comparable in all segments except within segment C3 where they are somewhat less negative, which begs the question concerning the possible causes for the higher isotopic values observed in this study. Given that the environment of deposition of the Cuchía sequence is delta influenced, we postulate that the variations observed arise from the averages of combined effects of modulated global factors due to the diverse OM from a complex ecosystem that developed in the basin.

A cursory review of the mechanism of carbon metabolic absorption will help to better understand the complexity of the carbon fractionation process and how it may have affected the residual OM preserved in the Cuchía sediments. It is generally accepted that $\delta^{13}C_{org}$ values depend on the different pathways of C-sequestration which are critical to the ratio obtained as an endmember of the photosynthetic process. In this relation, varying kinetic fractionation of $\delta^{13}C_{org}$ develops during photosynthesis. Basically, when terrestrial plants utilize atmospheric CO_2, they preferentially absorb the lighter ^{12}C which is easier to metabolize than ^{13}C because of their relative differential masses. Fractionation is further influenced by the photosynthetic pathway of carbon as plants may utilize the Calvin Cycle and they are designated C_3 plants because the CO_2 is initially fixed into a compound that contains three carbon atoms (phosphoglyceric acid) before entering the Calvin cycle. Terrestrial C_3 plants have $\delta^{13}C_{org}$ compositions more depleted in ^{13}C, yielding lower values of −22‰ to −33‰, generally averaging between −26‰ and −28.5‰ (Bender, 1971; Boutton, 1991; and others); they are interpreted as more negative, or with lower isotopic values. Climatic factors can also affect the carbon isotope values, as for instance, dominant C_3 plants in the present Gangetic plain (India) yield $\delta^{13}C_{org}$ values from −27‰ to −31.4‰, ($\bar{x}$=−28.9‰ ± 1.1‰), which decrease with increasing mean annual precipitation (Basu et al., 2015). Certain plants may also use the Hatch-Slack pathway where the CO_2 forms a simple 4-carbon organic compound (Oxaloacetic acid), classified as C_4 plants; this fractionation leads to higher $\delta^{13}C$ values in the −10‰ to −20‰ range (Bender, 1971). However, Bowes et al. (2002) hypothesized that aquatic C_4 photosynthesis possibly arose before its onset in terrestrial plants, and fossil plants indicate that C_4 plants originated much later, in the Paleogene Period, ~34—24 Ma (Sage, 2004). Therefore, contribution from C_4 plants can be ruled out as an enhancement factor for the higher $\delta^{13}C_{org}$ isotopic values in the Cuchía carbon isotopic archive. Thus, the enhancement factor of the carbon isotopic values in the Cuchía organic record must lie within the OM supplied by terrestrial C_3 photosynthesizers.

In this context, the remaining issue to be clarified in the Cuchía deposit is the photosynthetic mechanism that may have generated more positive $\delta^{13}C_{org}$ values from OM of C_3 photosynthesizers. The C_3 metabolic pathway with direct atmospheric-sourced CO_2, aquatic plants and marine algae acquire carbon from dissolved inorganic carbon (DIC), usually in the form of dissolved CO_2 or HCO_3^- (White, 2013). In this case, $^{13}CO_2$ dissolves more readily than $^{12}CO_2$ yielding a fractionation of about +0.9‰. Further fractionation of +7‰ to +8‰ occurs during hydration and dissociation of H_2CO_3, which also enriches ^{13}C in the DIC (White, 2013). Since the Cuchía section is a marine deposit, the OM is most likely derived predominately from pelagic *in situ* phyto- and zooplankton. But, the long chain *n*-alkanes and elevated TAR values (Figure 7) indicate that it was also strongly influenced by a delta (Rat, 1988), thus implying that riverine fluxes contributed to land-sourced OM which tend to have lower isotopic values. However, contrary to what would be expected, the carbon isotope negative excursion during C3 in Cuchía is not as pronounced as it is elsewhere (Figure 10). This anomaly can be explained because previous palynologic study of the section reveals the presence of gymnosperms (Najarro et al., 2011b). Indeed, modern aquatic analogs have shown that the carbon isotopic content for pond cypress trees (*Taxodium ascendens*) appears to respond to changes in precipitation, and more positive $\delta^{13}C_{org}$ values correlated with higher precipitation, yielding carbon isotopic values between −21.77‰ and −20.65‰ (Anderson et al., 2005). It is well demonstrated that the time associated with OAE1a was characterized by increased precipitation (e.g., Barron et al., 1981; Barron et al., 1995; Sanchez-Hernandez and Maurrasse, 2016 and others), accordingly we can surmise that such climatic conditions may have also affected the metabolic processes of the Aptian gymnosperms as observed in the present, which may explain the cause of the discrepancy in the record showing higher carbon isotopic values in the sedimentary archive of the Cuchía section.

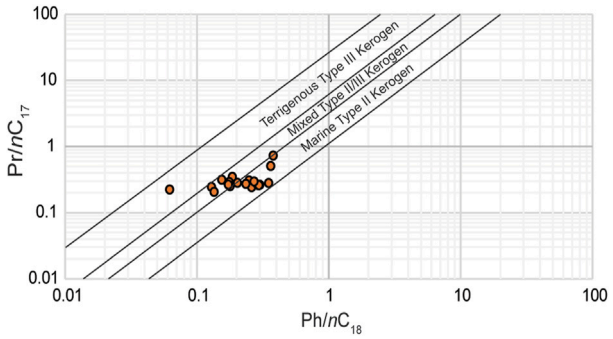

FIGURE 9
Cross plot of Pristane/*n*-C_{17} *versus* Phytane/*n*-C_{18} of selected samples for OM sources. The fields were first defined after Shanmugam (1985) from concepts proposed by Lijmbach (1975).

5.5 Influence of increased hydrological cycles on terrestrial fluxes in the NBCB

It has been well documented that the OAE interval is characterized by increased weathering rates and terrestrial fluxes due to enhanced precipitation, but how did the global greenhouse climate affect the supply of the terrigenous component in the expression of OAE1a in the delta influenced NBCB? This issue is addressed by measuring the temporal variability of the major elements (Al, Si, Ti), the clay and bulk mineral distributions, biophile elements (P, Fe), and the RSTEs because they can be used to infer periods of enhanced precipitation as their main delivery mechanism as well as productivity and the redox conditions at the time of deposition.

5.5.1 Significance of enhanced terrigenous input into the NBCB

Lithophile elements (Al, Si, and Ti) are frequently used to determine the magnitude of terrigenous fluxes into marine sedimentary basins because they are not involved in biomineralization (e.g., Murphy et al., 2000; Sanchez-Hernandez and Maurrasse, 2014; 2016; Socorro and Maurrasse, 2019; Zhang et al., 2019). Aluminum and Ti are conservative elements, mostly unaffected by biological processes and diagenesis, they are primarily sourced by fluvial and eolian detritus (Brumsack, 2006). In the Cuchía section the highest Al and Ti contents are observed in the

sediments with lower TIC content (r = −0.95 and r= −0.97, respectively) which correspond to the calcareous shale and shale intervals (Figures 4A,C). Titanium is strongly correlated with Al (r = 0.96); hence we can assume that it most likely originated from the adjacent Variscan terranes (Abalos et al., 2002). Silicon content may be modulated by biological processes due to biomineralization as amorphous opaline silica in a variety of organisms (diatoms, radiolaria, silicoflagellates, sponges) which are absent in the section, and since Si correlates positively with Al (r = 0.95) therefore it implies an increased delivery from common terrigenous source during periods of increased precipitation.

Similarly, clays are also detrital minerals that can shed light on their source area and their climatic conditions (Wilson, 1999; Sangüesa et al., 2000; Ruffell et al., 2002; Meunier, 2005; Prietzel et al., 2007; Pauly et al., 2013). They enter a sedimentary basin as residual minerals and can be transported over long distances without alteration remaining mostly unmodified within their depositional environments, or in burial <500 m (Weaver, 1958; Biscaye, 1965; Eslinger and Hsueh-Wen, 1981; Weaver, 1989; Wilson, 1999), therefore they are excellent proxies to indicate environmental conditions at the source and diagenetic transformation after burial. The clay fraction throughout the studied Cuchía section is dominated by illite with values ranging between 65% and 77% (Figure 6B). Illite typically derive from eroding low-grade metamorphic rocks and shales (Biscaye, 1965), but can be formed in natural environments indicative of dry climatic conditions (Chamley, 1989; Meunier, 2005; Sheldon and Tabor, 2009; Zhao et al., 2018). Illite can also form through burial diagenesis of smectite to mixed-layer illite/smectite (I/S), known as smectite illitization at temperature ~100—110°C (Hower et al., 1976; Deer et al., 1977; Hoffman and Hower, 1979; Eslinger and Pevear, 1985; Burtner and Warner, 1986; Scott, 1992; Cuadros and Linares, 1996; Du et al., 2019; McIntosh et al., 2021). At Cuchía, illite shows neither systematic increase with depth nor inverse relation to smectite which varies only from 1% to 4% (Figure 6B) and does not show any orderly change with depth, thus corroborating minimal diagenetic effect and low thermal maturity as indicated by CPI and OEP (2) values (Table 3). The consistent high relative temporal abundance of illite with respect to the other clay minerals throughout the studied section also implies a predominantly detrital origin (Weaver, 1958).

The chlorite group, which includes chamosite, may share a common origin with illite from weathered and low-grade metamorphosed rocks with mafic minerals and other weathered igneous rocks by the alteration of mafic minerals (Deer et al., 1977). Authigenic chlorite may also form as pressure and temperature increase through the alteration of other clay minerals (Ferry et al., 1983; Sangüesa et al., 2000). The relative abundance of chlorite in Cuchía fluctuates irregularly between 7% and 11% with no increase with depth (Figure 6B) thus considering that the CPI and the OEP (2) values discussed previously (*cf.* Section 5.6) indicate temperatures within the range of oil window (60—150°C) we infer that chlorite, like illite, originated from weathered adjacent landmasses.

Kaolinite is also of detrital origin indicative of warm and humid climatic conditions. It is predominantly the final weathering product of feldspars and diverse aluminum silicates from continental terranes (Biscaye, 1965; Curtis, 1983; Sangüesa et al., 2000; Sheldon and Tabor, 2009; Zhao et al., 2018). In the Cuchía section it is relatively stable with values fluctuating from 11% to 21% (Figure 6B), and its continuous occurrence is compatible with climatic conditions known to be associated with OAE1a (Barron and Washington, 1985; Huber et al., 1995; 2018Kuhnt et al., 2011).

In summary, the major elements concurrently with the average measured bulk mineralogy, which shows highest abundance of quartz (42%), feldspars (11%), and clay minerals (17%; Figure 6C) in the NBCB during OAE1a also reflect the global increase of terrigenous fluxes.

5.5.2 Source of biophile elements

Because the Cuchía site was delta influenced, it was more susceptible to be directly affected by weathering and enhanced precipitation that would have also intensified the supply of biophile elements as recorded in neighboring basins (Sanchez-Hernandez and Maurrasse, 2014; Socorro and Maurrasse, 2020).

Iron (Fe) being the predominant siderophile and fourth most abundant element in the Earth's crust it is expected to be prevalent in primary rock-forming minerals. As a result, it is naturally widespread in secondary phases of weathering mafic minerals into iron oxides or clay minerals (Prietzel et al., 2007; Muñoz et al., 2013; Simonnin et al., 2017). It is needed because of its ability to transfer electrons (synthesis of chlorophyll for photosynthesis, bacterial metabolic enzymes, and others); therefore, it is non-conservative. Iron's availability has been linked to productivity and the biogeochemical cycle in the marine environment. Hence, Fe is often used as a paleoproductivity proxy because it is one of the critical elements for primary producers (diazotrophic cyanobacteria or nitrogen-fixing bacteria) (Brand, 1991; Chappell et al., 2012). This biologically critical element would have been part of the Lower Cretaceous Ocean ecosystems. The presence of Fe in the Cuchía sediments shows temporal variations and moderate correlation with TOC (r = 0.52, R^2 = 0.27; Figure 11E), its correlation with Al is stronger (r = 0.71, R^2 = 0.50), and its highest values occur at levels with low TIC such as calcareous shale and shale. Hence, the distribution of Fe in Cuchía suggests a relationship with terrigenous sources. Thus, coeval increase or higher Fe content in the Cuchía section with levels of enhanced terrigenous fluxes (Figure 4) suggests two possible explanations associated with mineral byproducts. One could be ferric illite (Kossovskaya and Drits, 1970) being produced predominately in salt lakes or lagoons (Porrenga, 1968; Baker, 1997), although it is also believed to be formed in arid soils (Wilson, 1999; Meunier, 2005). The other possibility is from either smectite such as montmorillonite, or micas because they are the most iron bearing phyllosilicates from the terrigenous components (Simonnin et al., 2017). Non-etheless, because micas are missing in the studied Cuchía sediments, the excess Fe is most likely from ferric montmorillonite (Meunier, 2005). Since Fe shares a moderate correlation with TOC in the Cuchía section (Figures 4G, 11E), thus the sustained detrital Fe influx into the basin appears to be bonded to clays therefore it had limited availability to the biosphere and in productivity.

Inorganic Phosphorus (P) or orthophosphate (PO_4^{3-}), which is readily soluble, is the active P used in the metabolism of the living ecosystem and stimulates productivity. It is delivered to the ocean from chemical weathering of phosphatic rocks (Filippelli, 2008)

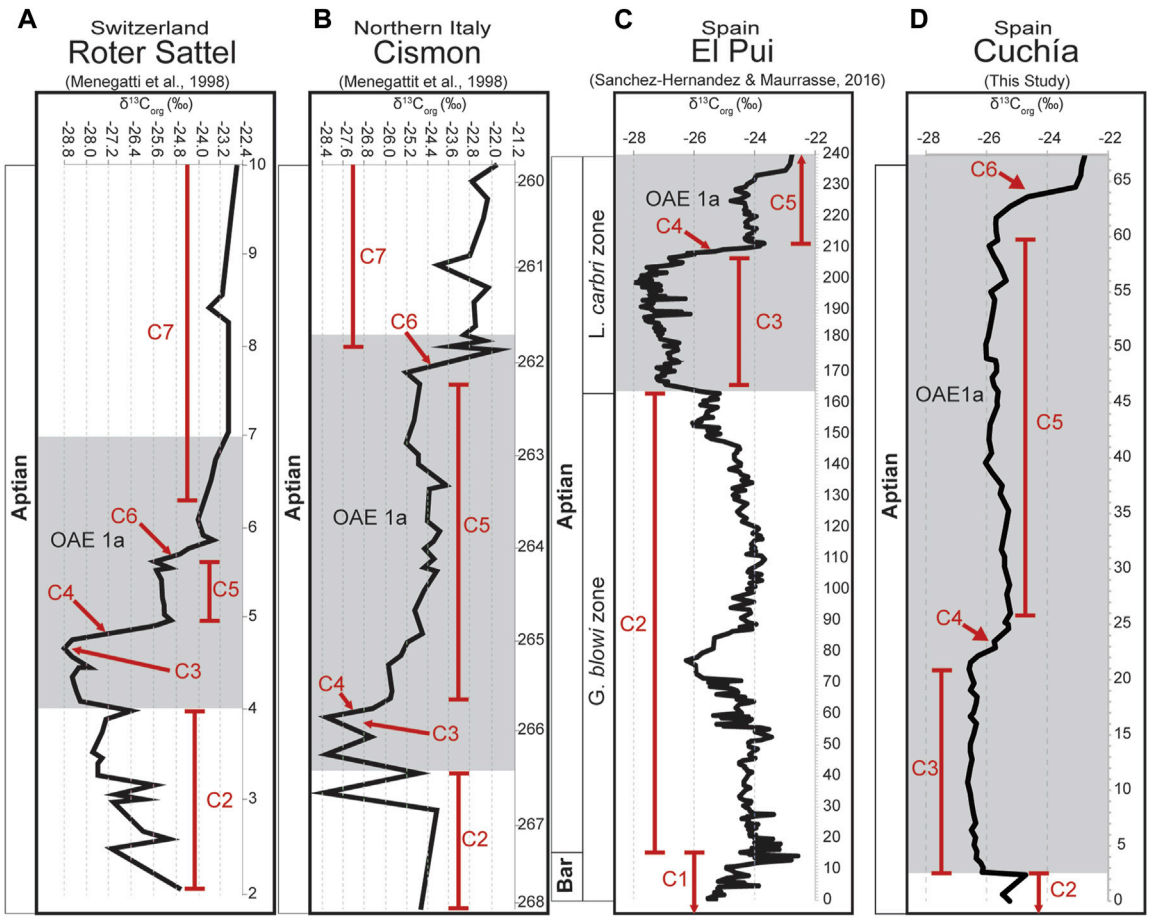

FIGURE 10
Chemostratigraphic correlation determined by the $\delta^{13}C_{org}$ comparing **(A)** the Roter Sattel, **(B)** the Cismon section (Menegatti et al., 1998), and **(C)** the El Pui section (Sanchez-Hernandez and Maurrasse, 2016) with **(D)** the Cuchía section (this study).

mostly under moist-warm climatic conditions (Föllmi, 1996; Delaney, 1998; Huang et al., 2012). Phosphorus is essential because it is an element pervasive in OM such as the soft decomposable tissue of both autotrophs and heterotrophs at all trophic levels, thus it is a key component to raise and sustain productivity from the base of the food chain upward (Martiny et al., 2019). Concerning terrigenous origin, the inorganic P The decay of OM enhances P adsorbed to iron-(oxy)hydroxides to the sediment where preservation is enhanced in clay-organic complexes that further refrain from microbial degradation (Pinck and Allison, 1951). Our results show that P does not appear to correlate with TOC (r = −0.01, R^2= 0.06; Figure 11D) or with Al (r = −0.21, R^2 = 0.04) and the Pearson correlation between P and TIC is r = 0.24, indicate that they do not seem to be strongly correlated either. P distribution is also decoupled from Fe (Figures 4F,G); therefore, its presence does not seem to be strongly associated with adsorption to Fe-oxides [Fe (OOH)] (Golterman, 1995; Golterman, 2001). The effects of long exposure of the outcrop to present enhanced pluvial weather and sea spray in the area may be invoked as a possible cause inducing diagenetic remobilization that may have affected the P record in the sediment which requires further studies (e.g., Puttonen et al., 2016).

5.5.3 Terrigenous fluxes regarding redox conditions in the NBCB during OAE1a

Terrigenous material is an important carrier of the RSTEs originating from the breakdown of continental crust and delivered by riverine fluxes (Scott et al., 2008). Being largely conservative elements, their preservation in the sediments depends on the redox conditions. The use of RSTEs as redox proxies relies on the evidence that under reducing conditions these elements may form organometallic-complexes, be adsorbed to Fe and/or Mn oxide and (oxy)hydroxide particles, or precipitate as minerals, thereby enriching their concentrations in the sediments. Conversely, under oxygenated conditions the RSTEs are mostly soluble and are enriched in the water column (Tribovillard et al., 2005; Siebert et al., 2006; Pattan and Pearce, 2009). In marine settings these trace metals are typically present as detritus material or as dissolved ions (Calvert and Pedersen, 1993; Achterberg et al., 1997). Typically, authigenic precipitation of RSTEs associated with OM-rich sediments are indicative of reducing conditions in the water column or at the sediment-water interface (Calvert and Pedersen, 1993; Jones and Manning, 1994; Morford et al., 2001; Rimmer, 2004; Tribovillard et al., 2004). Therefore, to interpret the degree of redox conditions, only the

authigenic fraction should be considered. Most authors remove the detrital fraction by normalizing the RSTE concentration to Al, which is achieved by dividing each amount of RSTE by the Al content, thus removing the terrigenous signal. Based on this information the normalized RSTE values are compared to the average shale value (Turekian and Wedepohl, 1961; Wedepohl, 1991; Brumsack, 2006) and generally correlations are made between the RSTEs and TOC to assess the redox conditions and/or to draw conclusion about common sources of these trace elements. Although this seems straightforward, this method of determining the redox conditions or the commonality between normalized concentrations of trace elements may require some caution. Indeed, Pearson (1896) and Van der Weijden (2002) explained in detail the drawbacks of normalization using a common divisor. Van der Weijden (2002) demonstrated that when variables are normalized, false or "spurious" correlation may arise between two elements that either share a positive correlation, a negative correlation, or no correlation before normalization. In contrast to these false correlations, Van der Weijden (2002) also proved how a positive correlation between two elements can be lost after normalization. This issue is related to the coefficient of variance (standard variation divided by the mean) between the numerator (trace metal) and the divisor (typically Al or Ti). When Al and/or Ti have a high coefficient of variance, false correlations between the trace elements being compared are formed and becomes more apparent as the coefficient of variance for these major elements increase. On the other hand, if Al or Ti have a low coefficient of variance or have a much lower coefficient of variance than the measured trace elements, spurious correlations will not form and will retain similar correlations values to the non-normalized trace elements. Thus, although spurious correlations have been shown to arise through normalization (Socorro and Maurrasse, 2019), nevertheless, in some cases normalization does not create false correlations (Sanchez-Hernandez and Maurrasse, 2016). Because Al and Ti contents have a high coefficient of variance (Al, v = 0.39; Ti, v = 0.34), in the case of this study the elemental concentrations of RSTEs are not normalized to avoid inaccurate correlation. Instead, the RSTE absolute values are used to assess the paleoredox conditions. Pearson correlations and cross-plots between the most significant RSTEs (V, Mo, U) and biolimiting trace metals (P, Fe), *versus* Al are used to further characterize the relationship of these elements and their possible provenance regarding terrigenous fluxes (Figure 12) as follows.

Vanadium (V) is an important proxy for paleoredox evaluation because under oxygenated conditions, it is found as soluble V(V) vanadate oxyanions ($H_2VO_4^-$ and HVO_4^{2-}) and adsorbed to Mn and Fe (oxy)hydroxides (Morford and Emerson, 1999; Hua et al., 2013), whereas it reduces to V(IV) in low oxygen environments, forming insoluble $VO(OH)_2$, and further reduces to V(III) in euxinic conditions forming as solid V_2O_3 and $V(OH)_3$ (Hua et al., 2013). In the Cuchía sediments V/Cr ratios show values consistently below 2 but above 1 (Figure 5F), which implies low oxygen conditions, but not reaching anoxia (Jones and Manning, 1994; Hetzel et al., 2009). Furthermore, V has a positive correlation with Al (r = 0.94; R^2 = 0.88; Figure 11F) and shows concurrent increase at the levels of calcareous shale and shale, thus implying a relationship with enhanced overland flows bringing terrigenous supply instead of being principally related to redox conditions. Indeed, Hatch and Leventhal (1992) argue that values between 0.54–0.82 indicate less strongly stratified anoxic water column. By comparison, in Cuchía V/(V+Ni) ratios stay between 0.60 and 0.79 (Figure 5E) which is compatible with the supply of V in relation to increased runoff that induced some degree of water column stratification.

Molybdenum (Mo) is supplied to the marine environment as dissolved molybdate anion (MoO_4^{2-}), originating from weathered porphyry-disseminated deposits in hydrothermal stockworks mostly related to basaltic and granitic rocks (1.5—1.0 ppm) (Table 2 in Turekian and Wedepohl, 1961; Scott et al., 2008). Despite its small amount in the ocean water, its low biological uptake (Collier, 1985) leads to its conservative property with a long residence time in the marine setting (7.6×10^5 years, Sohrin et al., 1998; ~500—750 Kyr; Akintomide et al., 2021), hence it is relatively one of the most well-supplied trace metals (~10 ppm) in present oceans (Anbar, 2004; Scott et al., 2008). Mo anions are insoluble in deoxygenated waters, therefore authigenic enrichment in sediments is primarily linked to reducing conditions (Brumsack, 2006; Scholz et al., 2013), and enrichment in the sediment is associated with sulphate reduction in euxinic environments in the presence of H_2S (Helz et al., 2011). In Cuchía, Mo is poorly correlated with TOC (R^2 = 0.01; Figure 11G) and Al (R^2 = 0.09; Figure 12F) and is decoupled from Fe (Figure 4G; 5F), therefore other factors may be involved because both Fe and OM are the scavenging agents (Helz et al., 1996). However, the increase in Mo concurrent with the onset of positive CIE segment C4 transitioning into C5 between ~26 m and 29 m (Figure 3D; Figure 5C) is consistent with a minor reducing condition and Mo sorbing on Fe and Mn due to a transient episode of decreased terrigenous flux (Dumitrescu et al., 2006; Kuhnt et al., 2011; Sanchez-Hernandez and Maurrasse, 2016).

Uranium (U) originates from sedimentary and mostly granitic rocks of the Earth's crust. It is released by weathering processes and delivered to the ocean *via* runoff as a trace element (~99% U-238). It is a large ion lithophile element (small charge to ionic radius; Gast, 1972) which is present in low concentration in seawater (~3ppb) as U(VI) and is soluble under oxic conditions. Uranium forms complexes with carbonate ions to form $[UO_2(CO_3)_3]^{4-}$ or occurs as a free uranyl ion (UO_2^{2+}) (Morford and Emerson, 1999), but under reducing conditions U(VI) is not thermodynamically reduced to U(IV) or scavenged by particulates. The reduction of U and its removal occurs as it diffuses into the sediment where oxygen is deficient and is reduced to U(IV) at the Fe(II)-Fe(III) redox boundary. In its reduced form, U(IV) is preserved in the sediment through adsorption or precipitation as uraninite (UO_2) (Emerson and Huested, 1991). In Cuchía U has a moderate correlation with TOC (r = 0.51 and R^2 = 0.26, Figure 11H) whereas its relationship with Al (r = 0.76; R^2 = 0.58; Figure 12G) is stronger, again implying that the increase of this RSTE is not tied to deoxygenation but has a detrital origin.

In summary, determinant RSTEs (V, Mo, U) have a disparate temporal distribution relative to TOC in the Cuchía section, therefore they may not be directly bonded to the OM and thus apparently concur with a terrigenous origin and their increase are not due to severe oxygen deficiency. Instead, most RSTEs have a strong relationship with Al, which supports their presence in the basin *via* terrestrial fluxes compatible due to overland flow associated with increased precipitation.

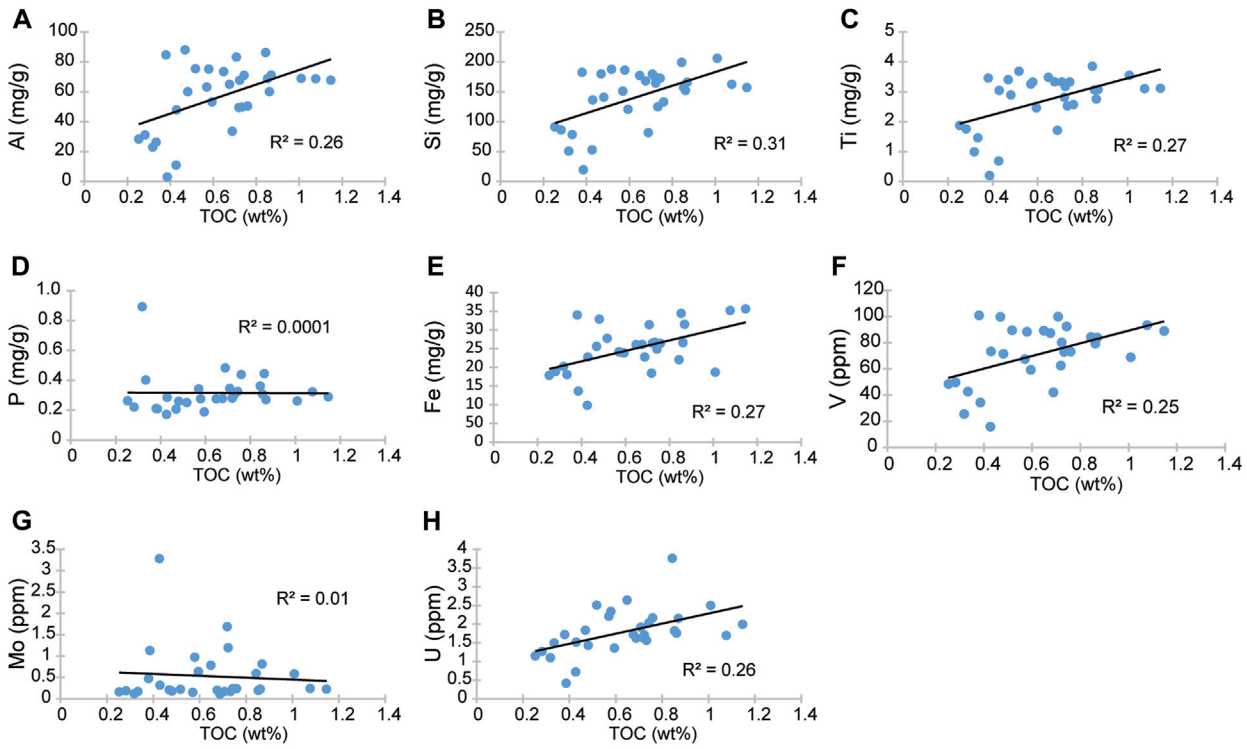

FIGURE 11
Linear crossplots TOC, showing the correlation coefficient (R^2). **(A)** Aluminum; **(B)** silicon; **(C)** titanium; **(D)** phosphorous; **(E)** iron; **(F)** vanadium **(G)** molybdenum; **(H)** uranium.

5.5.4 Role of terrigenous input in the accumulation rate and absence of anoxic conditions in the preservation of OM

The RSTEs together with the terrigenous input indicate that the Cuchía section did not experience severe oxygen deficiency as a potential dominant factor in the basin, yet there is evidence of some OM preservation as observed elsewhere during OAE1a; therefore, the question arises regarding the forcing factors involved in the preservation OM in this part of the NBCB.

Based on the non-carbonate fraction, accumulation rates in the Cuchía succession can be attributed to mostly terrigenous input as indicated by Si which is of terrestrial origin because it correlates strongly with Al (r = 0.95) as observed in modern analog environments (Wei et al., 2022). *In-situ* production of carbonate by biomineralizers varies intermittently, such effects can be observed in many instances such as the TIC curve (Figure 3B), the variation of the major element Al (Figure 4C), and the TAR (Figure 7C). For instance, the average TIC within C3 is 14.1%, for C4 = 8.8%, and for C5 = 18.2% which will affect the temporal accumulation rate in the basin. The durations of the carbon isotope segments during OAE1a show highly variable sedimentation rates as could be expected. Segments C3 to C6 were calculated based on orbital cycles preserved at two sites: Cismon APTICORE in Italy and the Santa Rosa Canyon section in northeastern Mexico (Li et al., 2008). Their results assigned segment C3 a duration of 27–44 kyr, C4 lasted 330 kyr, C5 = 570 kyr, and C6 = 310–330 kyr. Because the Cismon section is either a condensed interval or is discontinuous (e.g., Li et al., 2008; Najarro et al., 2011b; Kuhnt et al., 2011; Castro et al., 2021), there is apparent underestimation for the C3 duration. By contrast, Kuhnt et al. (2011) estimated the duration of segment C3 at La Bédoule to >100 kyr by determining an average sedimentation rate of ~2.5–3.2 cm/kyr, based on a 32 m thickness of the section and a total duration of 1–1.3 Ma for OAE1a. Similarly, Lorenzen et al. (2013) estimated the duration of segment C3 by taking an average sedimentation rate of 1.6–2 cm/kyr over the whole Selli Level (C3-C6) from their LB1 core taken from La Bédoule (SE France). Their calculation yields a duration of 280–350 kyr for segment C3. Therefore, due to the uncertainty at the Cismon APTICORE, here we use the estimated durations (100–350 kyr) determined at La Bédoule (Kuhnt et al., 2011; Lorenzen et al., 2013) for segment C3 at the Cuchía section.

Our estimates of accumulation rates in the studied Cuchía section cover segments C3 to C5 which were completely sampled (Figure 3D). Hence, segment C3 with a thickness of 19.2 m, which yields a dry bulk sedimentation rate between 5.5 and 19.2 cm/kyr; C4 is 3.05 m thick thus gives a rate of 0.92 cm/kyr; and C5 which covers 37.11 m has a rate of 6.51 cm/kyr. These diverse estimates suggest that the highest accumulation rates occurred within segment C3 and C5 and the lowest rates within C4, which are consistent with other Tethyan sites elsewhere (e.g., Sanchez-Hernandez et al., 2014; Socorro and Maurrasse, 2022).

Since the different environmental proxies point to terrigenous supplies as the predominant forcing factor in the NBCB during OAE1a, it becomes understandable that OM preservation must be related to such processes. Indeed, continuous occurrence of high-molecular-weight *n*-alkanes throughout the section indicates

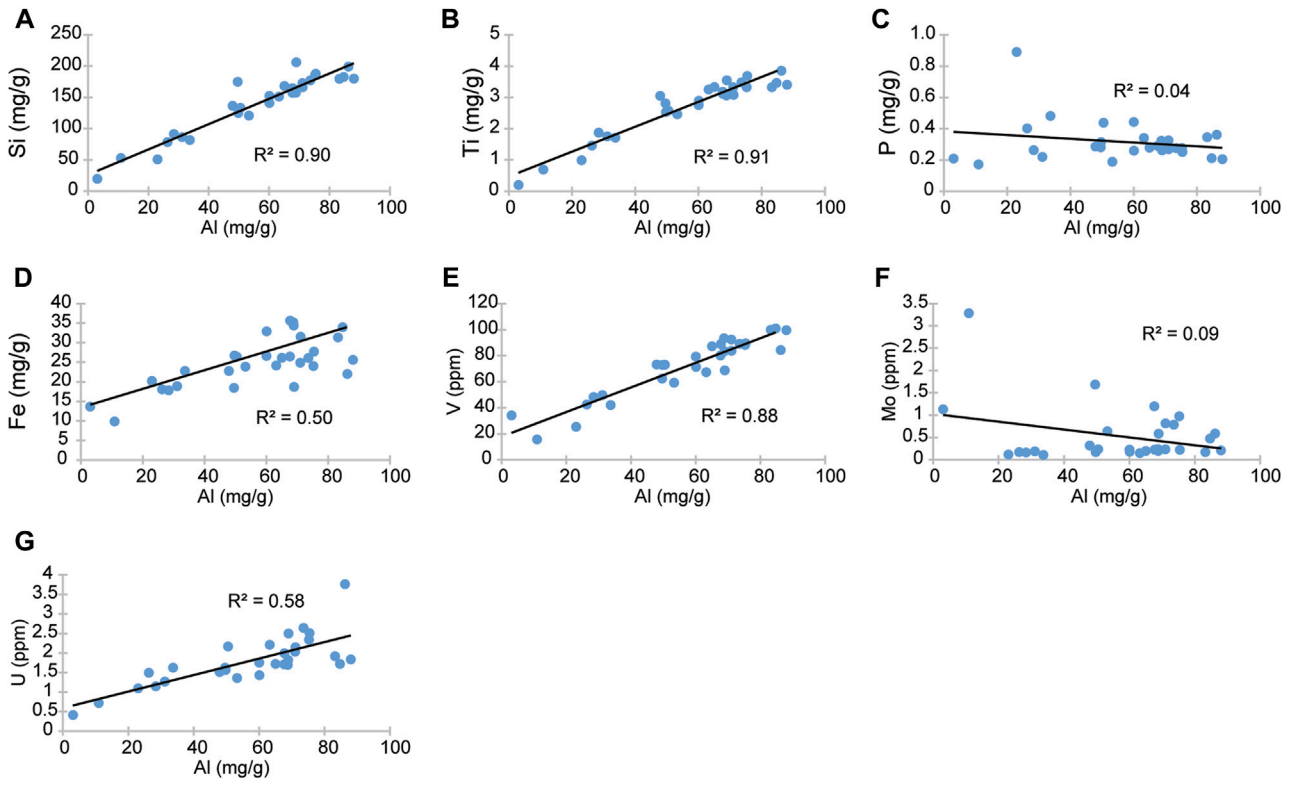

FIGURE 12
Linear crossplots of all measured trace elements *versus* Al, showing the correlation coefficient (R^2). **(A)** Silicon; **(B)** titanium; **(C)** phosphorous; **(D)** iron; **(E)** vanadium; **(F)** molybdenum; **(G)** uranium.

significant contribution of OM originating from terrestrial plants (Dañobeitia et al., 1990; Frakes et al., 1992; Kuhnt et al., 1998; de Gea et al., 2003; Forster et al., 2004). Because these long chain *n*-alkanes are more recalcitrant than their lower molecular weight counterparts (Head et al., 2006) this may further explain why OM was being preserved despite absence of anoxia. Furthermore, the high sedimentation rates during OAE1a may have heightened their preservation because rapid burial restricts OM remineralization, and the clays augment this process as illite can bind to charged organic compounds or non-charged compounds through Van der Waals bonding providing increased protection against microbial degradation (Keil and Mayer, 2014; Chen et al., 2018).

In essence, the interacting effects of terrestrial pulse associated with increased precipitation and the physiographic conditions of the NBCB controlled the accumulation rate and provided more recalcitrant land-derived OM which are more readily preserved. In addition, OM preservation was further facilitated by their interaction with land-sourced clay minerals.

6 Conclusion

The multi-proxy geochemical study carried out on the 67 m succession of the Cuchía section of the NBCB provided explicit evidence that further underscores the controlling influence of heightened terrigenous fluxes that led to unusual allowed for further characterization of the paleoenvironmental response to OAE1a within the NBCB. The carbon isotope curve corroborates the chronostratigraphic position of the section within carbon isotope segments C2 through C6, in concurrence with previous biostratigraphic studies. Differences in the amplitude of the carbon isotope values in the section are modulated by local factors such as terrestrially derived OM from gymnosperms of a deltaic environment during a period of increased precipitation. The modulating effects of this allochthonous OM induced a less pronounced negative excursion within carbon isotope segment C3.

Most RSTEs covary strongly with Al and show a disparate temporal distribution relative to TOC, which suggests that they are of terrigenous origin and indicate that the basin did not reach severe oxygen deficient conditions. Heightened terrigenous fluxes increased sedimentation rates and provided the less labile terrestrial OM which facilitated their accumulation and preservation. Interaction between the clay minerals and the OM further bolstered their preservation.

This study of the NBCB provides the geochemical data that further clarify the influence on the long-term combined effects of weathering and increased precipitation associated with greenhouse climate which triggered the environmental response that developed during OAE1a.

Data availability statement

The original contributions presented in the study are included in the article/Supplementary Material, further inquiries can be directed to the corresponding author.

Author contributions

CH: Conceptualization, Field sampling, Formal analysis, Data curation, Writing–original draft, Writing–review and editing. FJ-MM: Supervision, Data curation, Writing–original draft, Writing–review and editing. The authors have made a substantial, direct, and intellectual contribution to the work, and have read and approved it for publication.

Funding

This research was funded by the Glenn A. Goodfriend Memorial Fund.

Acknowledgments

We gratefully acknowledge Diane Pirie for her help with materials at FIU. We are grateful to Josep Moreno-Bedmar and the late Prof. Marcos Lamolda for the initial reconnaissance of the site. We thank our colleague Jander Socorro for assisting with fieldwork. The Earth and Environment Department at FIU generously provided us with supplies and other laboratory materials. We are grateful to Bill Anderson and John Harris for the carbon isotope analyses, Cesar Ramirez at FIU's Advanced Spectrometry Facility for the biomarker analyses, Martin Pentrak of Illinois State University for the XRD analysis, and Sarah Jantzi at FIU's Trace Evidence Analysis Facility (TEAF) for elemental analyses. CH is most grateful for the financial support provided by the Dissertation Year Fellowship (DYF) from the FIU Graduate School.

Conflict of interest

The authors declare that the research was conducted in the absence of any commercial or financial relationships that could be construed as a potential conflict of interest.

Publisher's note

All claims expressed in this article are solely those of the authors and do not necessarily represent those of their affiliated organizations, or those of the publisher, the editors and the reviewers. Any product that may be evaluated in this article, or claim that may be made by its manufacturer, is not guaranteed or endorsed by the publisher.

References

Abalos, B., Carreras, J., Druguet, E., Viruete, J. E., Gómez Pugnaire, M. T., Alvarez, S. L., et al. (2002). "Variscan and pre-variscan tectonics," in *The Geology of Spain*. Editors W. Gibbons and T. Moreno (London: J. Geol. Soc.), 155–183.

Abu-Zied, R. H. (2007). Palaeoenvironmental significance of early cretaceous foraminifera from northern sinai, Egypt. *Cretac. Res.* 28, 765–784. doi:10.1016/j.cretres.2006.11.002

Achterberg, E. P., van den Berg, C. M. G., Boussemart, M., and Davison, W. (1997). Speciation and cycling of trace metals in esthwaite water: A productive English lake with seasonal deep-water anoxia. *Geochimica Cosmochimica Acta* 61 (24), 5233–5253. doi:10.1016/S0016-7037(97)00316-5

Aguirre-Urreta, M. B., Price, G. D., Ruffell, A. H., Lazo, D. G., Kalin, R. M., Ogle, N., et al. (2008). Southern hemisphere early cretaceous (Valanginian-Early barremian) carbon and oxygen isotope curves from the neuquén basin, Argentina. *Cretac. Res.* 29, 87–99. doi:10.1016/j.cretres.2007.04.002

Akintomide, O. A., Adebayo, S., Horn, J. D., Kelly, R. P., and Johannesson, K. H. (2021). Geochemistry of the redox-sensitive trace elements molybdenum, tungsten, and rhenium in the euxinic porewaters and bottom sediments of the Pettaquamscutt River estuary, Rhode Island. *Chem. Geol.* 584, 120499. doi:10.1016/j.chemgeo.2021.120499

Anbar, A. D. (2004). Molybdenum stable isotopes: Observations, interpretations and directions. *Rev. Mineralogy Geochem.* 55, 429–454. doi:10.2138/gsrmg.55.1.429

Anderson, W. T., Sternberg, L. S. L., Pinzon, M. C., Gann-Troxler, T., Childers, D. L., and Duever, M. (2005). Carbon isotopic composition of cypress trees from South Florida and changing hydrologic conditions. *Dendrochronologia* 23, 1–10. doi:10.1016/j.dendro.2005.07.006

Arroyo, L., Trejos, T., Gardinali, P. R., and Almirall, J. R. (2009). Optimization and validation of a laser ablation inductively coupled plasma mass spectrometry method for the routine analysis of soils and sediments. *Spectrochim. Acta Part B At. Spectrosc.* 64, 16–25. doi:10.1016/j.sab.2008.10.027

Arthur, M. A., Brumsack, H.-J., Jenkyns, H. C., and Schlanger, S. O. (1990). in *Stratigraphy, geochemistry, and paleoceanography of organic carbon-rich cretaceous sequences" in:* Cretaceous resources, Events and rhythms: Background and Plans for research. Editors R. N. Ginsburg and B. Beaun (Dordrecht: Springer Netherlands), 75–119.

Arthur, M. A., Dean, W. E., and Schlanger, S. O. (1985). "Variations in the global carbon cycle during the Cretaceous related to climate, volcanism, and changes in atmospheric CO2," in *The carbon cycle and atmospheric CO2: Natural variations archean to present*. Editors W. S. Sundquist and W. S. Broecker (Washington, D.C: AGU, Advancing Earth and space science), 504–529.

Arthur, M. A. (1979). North atlantic cretaceous black shales: The record at site 398 and a brief comparison with other occurrences. *Initial. Rep. Deep Sea Drill. Proj.* 47 (2), 719–751. doi:10.2973/dsdp.proc.47-2.136.1979

Baker, J. C. (1997). Green ferric clay in non-marine sandstones of the Rewan Group, southern Bowen Basin, eastern Australia. *Clay Min.* 32 (4), 499–506. doi:10.1180/claymin.1997.032.4.01

Barragán, R., and Maurrasse, F. J.-M. R. (2008). Lower aptian (lower cretaceous) ammonites from the basal strata of the La peña formation of nuevo león state, northeast Mexico: Biochronostratigraphic implications. *Rev. Mex. Ciencias Geol.* 25, 145–157.

Barron, E. J., Fawcett, P. J., Peterson, W. H., Pollard, D., and Thompson, S. L. (1995). A "simulation" of Mid-Cretaceous climate. *Paleoceanography* 10, 953–962. doi:10.1029/95PA01624

Barron, E. J., Harrison, C. G. A., Sloan, J. L., and Hay, W. W. (1981). Paleogeography, 180 million years to present. *Eclogae Geol. Helv.* 74, 443–470.

Barron, E. J., and Washington, W. M. (1985). "Warm cretaceous climates: High atmospheric CO2 as a plausible mechanism," in *The carbon Cycle and atmospheric CO2: Natural variations Archean to present*. Editors W. S. Sundquist and W. S. Broecker (Washington, D.C: AGU, Advancing Earth and space science), 546–553.

Basilone, L., Perri, F., Sulli, A., and Critelli, S. (2017). Paleoclimate and extensional tectonics of short-lived lacustrine environments. Lower Cretaceous of the Panormide Southern Tethyan carbonate platform (NW Sicily). *Mar. Petroleum Geol.* 88, 428–439. doi:10.1016/j.marpetgeo.2017.08.041

Basu, S., Agrawal, S., Sanyal, P., Mahato, P., Kumar, S., and Sarkar, A. (2015). Carbon isotopic ratios of modern C3–C4 plants from the Gangetic Plain, India, and its implications to paleovegetational reconstruction. *Palaeogeogr. Palaeoclimatol. Palaeoecol.* 440, 22–32. doi:10.1016/j.palaeo.2015.08.012

Bellanca, A., Erba, E., Neri, R., Premoli Silva, I., Sprovieri, M., Tremolada, F., et al. (2002). Palaeoceanographic significance of the tethyan 'livello Selli' (early aptian) from the hybla formation, northwestern sicily: Biostratigraphy and high-resolution chemostratigraphic records. *Palaeogeogr. Palaeoclimatol. Palaeoecol.* 185, 175–196. doi:10.1016/S0031-0182(02)00299-7

Bender, M. M. (1971). Variations in the $^{13}C/^{12}C$ ratios of plants in relation to the pathway of photosynthetic carbon dioxide fixation. *Phytochemistry* 10, 1239–1244. doi:10.1016/S0031-9422(00)84324-1

Biscaye, P. E. (1965). Mineralogy and sedimentation of recent deep-sea clay in the Atlantic Ocean and adjacent seas and oceans. *Geol. Soc. Am. Bull.* 76, 803–832. doi:10.1130/0016-7606(1965)76[803:MASORD]2.0.CO;2

Bourbonniere, R. A., and Meyers, P. A. (1996). Sedimentary geolipid records of historical changes in the watersheds and productivities of Lakes Ontario and Erie. *Limnol. Oceanogr.* 41, 352–359. doi:10.4319/lo.1996.41.2.0352

Boutton, T. W. (1991). "Stable carbon isotope ratios of natural materials ii atmospheric terrestrial marine and freshwater environments," in *Carbon isotope techniques*. Editors D. C. Coleman and B. Fry (San Diego, California: Academic Press), 173–186.

Bowes, G., Rao, S. K., Estavillo, G. M., and Reiskind, J. B. (2002). C4 mechanisms in aquatic angiosperms: Comparisons with terrestrial C4 systems. *Funct. Plant Biol.* 29 (3), 379–392. doi:10.1071/pp01219

Brand, L. E. (1991). Minimum iron requirements of marine phytoplankton and the implications for the biogeochemical control of new production. *Limnol. Oceanogr.* 36, 1756–1771. doi:10.4319/lo.1991.36.8.1756

Bray, E. E., and Evans, E. D. (1961). Distribution of n-paraffins as a clue to recognition of source beds. *Geochimica Cosmochimica Acta* 22, 2–15. doi:10.1016/0016-7037(61)90069-2

Brumsack, H.-J. (2006). The trace metal content of recent organic carbon-rich sediments: Implications for cretaceous black shale formation. *Palaeogeogr. Palaeoclimatol. Palaeoecol.* 232, 344–361. doi:10.1016/j.palaeo.2005.05.011

Burtner, R. L., and Warner, M. A. (1986). Relationship between illite/smectite diagenesis and hydrocarbon generation in lower cretaceous mowry and skull creek shales of the northern rocky mountain area. *Clays Clay Minerals* 34, 390–402. doi:10.1346/CCMN.1986.0340406

Calvert, S. E., and Pedersen, T. F. (1993). Geochemistry of recent oxic and anoxic marine sediments: Implications for the geological record. *Mar. Geol.* 113, 67–88. doi:10.1016/0025-3227(93)90150-T

Capote, R., Muñoz, J. A., Simón, J. L., Liesa, C. L., and Arlegui, L. E. (2002). "Alpine tectonics I: The alpine system north of the betic cordillera," in *The Geology of Spain*. Editors W. Gibbons and T. p. Moreno (McLean, United States: GeoScienceWorld), 367–400.

Castro, J. M., Ruiz-Ortiz, P. A., de Gea, G. A., Aguado, R., Jarvis, I., Weissert, H., et al. (2021). High-resolution C-isotope, TOC and biostratigraphic records of OAE1a (aptian) from an expanded hemipelagic cored succession, Western tethys: A new stratigraphic reference for global correlation and paleoenvironmental reconstruction. *Paleoceanogr. Paleoclimatol.* 36, e2020PA004004. doi:10.1029/2020PA004004

Chaler, R., Dorronsoro, C., Grimalt, J. O., Agirrezabala, L. M., Fernández-Mendiola, P. A., García-Mondejar, J., et al. (2005). Distributions of C22–C30 even-carbon-number n-alkanes in ocean anoxic event 1 samples from the Basque-Cantabrian Basin. *Naturwissenschaften* 92, 221–225. doi:10.1007/s00114-005-0616-2

Chamley, H. (1989). "Clay formation through weathering," in *Clay sedimentology* (Berlin, Germany: Springer), 21–50.

Channell, J. E. T., and Erba, E. (1992). Early Cretaceous polarity chrons CM0 to CM11 recorded in northern Italian land sections near Brescia. *Earth Planet. Sci. Lett.* 108, 161–179. doi:10.1016/0012-821X(92)90020-V

Channell, J. E. T., Erba, E., Muttoni, G., and Tremolada, F. (2000). Early Cretaceous magnetic stratigraphy in the APTICORE drill core and adjacent outcrop at Cismon (Southern Alps, Italy), and correlation to the proposed Barremian-Aptian boundary stratotype. *Geol. Soc. Am. Bull.* 112, 1430–1443. doi:10.1130/0016-7606(2000)112<1430:ECMSIT>2.0.CO;2

Chappell, P. D., Moffett, J. W., Hynes, A. M., and Webb, E. A. (2012). Molecular evidence of iron limitation and availability in the global diazotroph Trichodesmium. *ISME J.* 6, 1728–1739. doi:10.1038/ismej.2012.13

Chen, S., Hong, H., Huang, X., Fang, Q., Yin, K., Wang, C., et al. (2018). The role of organo-clay associations in limiting organic matter decay: Insights from the Dajiuhu peat soil, central China. *Geoderma* 320, 149–160. doi:10.1016/j.geoderma.2018.01.013

Choukroune, P., Le Pichon, X., Seguret, M., and Sibuet, J.-C. (1973). Bay of Biscay and pyrenees. *Earth Planet. Sci. Lett.* 18, 109–118. doi:10.1016/0012-821X(73)90041-1

Coccioni, R., Luciani, V., and Marsili, A. (2006). Cretaceous oceanic anoxic events and radially elongated chambered planktonic foraminifera: Paleoecological and paleoceanographic implications. *Palaeogeogr. Palaeoclimatol. Palaeoecol.* 235, 66–92. doi:10.1016/J.PALAEO.2005.09.024

Collier, R. W. (1985). Molybdenum in the northeast pacific Ocean1. *Limnol. Oceanogr.* 30, 1351–1354. doi:10.4319/lo.1985.30.6.1351

Cranwell, P. A. (1973). Chain-length distribution of n-alkanes from lake sediments in relation to post-glacial environmental change. *Freshw. Biol.* 3, 259–265. doi:10.1111/j.1365-2427.1973.tb00921.x

Cranwell, P. A. (1981). Diagenesis of free and bound lipids in terrestrial detritus deposited in a lacustrine sediment. *Org. Geochem.* 3, 79–89. doi:10.1016/0146-6380(81)90002-4

Cranwell, P. A., Eglinton, G., and Robinson, N. (1987). Lipids of aquatic organisms as potential contributors to lacustrine sediments—II. *Org. Geochem.* 11, 513–527. doi:10.1016/0146-6380(87)90007-6

Cuadros, J., and Linares, J. (1996). Experimental kinetic study of the smectite-to-illite transformation. *Geochimica Cosmochimica Acta* 60, 439–453. doi:10.1016/0016-7037(95)00407-6

Curtis, C. D. (1983). Link between aluminum mobility and destruction of secondary Porosity1: Geologic notes. *Am. Assoc. Pet. Geol. Bull.* 67, 380–384. doi:10.1306/03B5AD22-16D1-11D7-8645000102C1865D

Dañobeitia, J. J., Alonso, B., and Maldonado, A. (1990). Geological framework of the Ebro continental margin and surrounding areas. *Mar. Geol.* 95, 265–287. doi:10.1016/0025-3227(90)90120-9

de Gea, G. A., Castro, J. M., Aguado, R., Ruiz-Ortiz, P. A., and Company, M. (2003). Lower aptian carbon isotope stratigraphy from a distal carbonate shelf setting: The cau section, prebetic zone, SE Spain. *Palaeogeogr. Palaeoclimatol. Palaeoecol.* 200, 207–219. doi:10.1016/S0031-0182(03)00451-6

Deer, W. A., Howie, R. A., and Zussman, J. (1977). *An introduction to the rock-forming minerals*. London, United Kingdom: Longman Publisher, 528.

Delaney, M. L. (1998). Phosphorus accumulation in marine sediments and the oceanic phosphorus cycle. *Glob. Biogeochem. Cycles* 12, 563–572. doi:10.1029/98GB02263

Dinarès-Turell, J., and Garcia-Senz, J. (2000). Remagnetization of Lower Cretaceous limestones from the southern Pyrenees and relation to the Iberian plate geodynamic evolution. *J. Geophys. Res. Solid Earth* 105, 19405–19418. doi:10.1029/2000JB900136

Du, J., Cai, J., Chen, Z., Lei, T., Zhang, S., and Xie, Z. (2019). A contrastive study of effects of different organic matter on the smectite illitization in hydrothermal experiments. *Appl. Clay Sci.* 168, 249–259. doi:10.1016/j.clay.2018.11.016

Dumitrescu, M., Brassell, S. C., Schouten, S., Hopmans, E. C., and Damsté, J. S. S. (2006). Instability in tropical Pacific sea-surface temperatures during the early Aptian. *Geology* 34, 833–836. doi:10.1130/G22882.1

Elkhazri, A., Abdallah, H., Razgallah, S., Moullade, M., and Kuhnt, W. (2013). Carbon-isotope and microfaunal stratigraphy bounding the lower aptian oceanic anoxic event 1a in northeastern Tunisia. *Cretac. Res.* 39, 133–148. doi:10.1016/j.cretres.2012.05.011

Emerson, S. R., and Huested, S. S. (1991). Ocean anoxia and the concentrations of molybdenum and vanadium in seawater. *Mar. Chem.* 34, 177–196. doi:10.1016/0304-4203(91)90002-E

Erbacher, J., and Thurow, J. (1997). Influence of oceanic anoxic events on the evolution of mid-Cretaceous radiolaria in the North Atlantic and Western Tethys. *Mar. Micropaleontol.* 30, 139–158. doi:10.1016/S0377-8398(96)00023-0

Eslinger, E., and Pevear, D. (1985). *Clay minerals for petroleum geologists and engineers*. McLean, United States: GeoScienceWorld.

Eslinger, E. V., and Hsueh-Wen, Y. (1981). Mineralogy, O18/O16, and D/H ratios of clay-rich sediments from deep sea drilling project site 180, aleutian trench. *Clays Clay Minerals* 29, 309–315. doi:10.1346/CCMN.1981.0290409

Feakins, S. J., Eglinton, T. I., and de Menocal, P. B. (2007). A comparison of biomarker records of northeast African vegetation from lacustrine and marine sediments (ca. 3.40 Ma). *Org. Geochem.* 38, 1607–1624. doi:10.1016/j.orggeochem.2007.06.008

Feakins, S. J., Peters, T., Wu, M. S., Shenkin, A., Salinas, N., Girardin, C. A. J., et al. (2016). Production of leaf wax n-alkanes across a tropical forest elevation transect. *Org. Geochem.* 100, 89–100. doi:10.1016/j.orggeochem.2016.07.004

Feinstein, S. (1981). Subsidence and thermal history of southern Oklahoma aulacogen: Implications for petroleum exploration. *AAPG Bull.* 65 (12), 2521–2533. doi:10.1306/03B599F9-16D1-11D7-8645000102C1865D

Ferry, S., Cotillon, P., and Rio, M. (1983). Diagenèse croissante des argiles dans des niveaux isochrones de l'alternance calcaire-marne valanginienne du bassin vocontien. Zonation géographique. C.R. Acad. Sci. *Paris, II* 297, 51–56.

Ficken, K. J., Li, B., Swain, D. L., and Eglinton, G. (2000). An n-alkane proxy for the sedimentary input of submerged/floating freshwater aquatic macrophytes. *Org. Geochem.* 31, 745–749. doi:10.1016/S0146-6380(00)00081-4

Filippelli, G. M. (2008). The global phosphorus cycle: Past, present, and future. *Elements* 4, 89–95. doi:10.2113/GSELEMENTS.4.2.89

Fletcher, B. J., Brentnall, S. J., Anderson, C. W., Berner, R. A., and Beerling, D. J. (2008). Atmospheric carbon dioxide linked with Mesozoic and early Cenozoic climate change. *Nat. Geosci.* 1, 43–48. doi:10.1038/ngeo.2007.29

Föllmi, K. B. (2012). Early Cretaceous life, climate and anoxia. *Cretac. Res.* 35, 230–257. doi:10.1016/J.CRETRES.2011.12.005

Föllmi, K. B. (1996). The phosphorus cycle, phosphogenesis and marine phosphate-rich deposits. *Earth-Science Rev.* 40, 55–124. doi:10.1016/0012-8252(95)00049-6

Forster, A., Sturt, H., and Meyers, P. A. (2004). *Molecular biogeochemistry of Cretaceous black shales from the Demerara rise: Preliminary shipboard results from sites 1257 and 1258, Leg 207*. Proc. Ocean Drill. Program Initial Rep., 207, 22.

Frakes, L. A., Francis, J. E., and Syktus, J. I. (1992). *Climate modes of the phanerozoic: The history of the earth's climate over the past 600 million years*. Cambridge: Cambridge University Press. doi:10.1017/CBO9

Gaona-Narvaez, T., Maurrasse, F. J-M. R., and Moreno-Bedmar, J. A. (2013). Stable carbon-isotope stratigraphy and ammonite biochronology at madotz, navarra, northern Spain: Implications for the timing and duration of oxygen depletion during OAE-1a. *Cretac. Res.* 40, 143–157. doi:10.1016/J.CRETRES.2012.06.005

García-Mondéjar, J., Fernández-Mendiola, P. A., and Owen, H. G. (2015a). The OAE1a in Cuchía (early aptian, Spain): C and O geochemistry and global correlation. *Acta Geol. Pol.* 65, 525–543. doi:10.1515/agp-2015-0023

García-Mondéjar, J., Owen, H. G., and Fernández-Mendiola, P. A. (2015b). Early Aptian sedimentary record and OAE1a in Cuchía (northern Spain): New data on facies and ammonite dating. *Neues Jahrb. für Geol. Paläontologie - Abh.* 276, 1–26. doi:10.1127/njgpa/2015/0466

García-Senz, J. (2002). "Cuencas extensivas del Cretácico Inferior en los Pirineos centrales," in *Formación y subsecuente inversión* (Barcelon, Spain: Universitat de Barcelona), 310.*[PhD dissertation]*

Gast, P. W. (1972). The chemical composition and structure of the moon. *Moon* 5, 121–148. doi:10.1007/BF00562108

Goddard, E. N., Trask, P. D., DeFord, R. K., Rove, O. N., Singewald, J. T., and Overbeck, R. M. (1984). *Rock color chart: Boulder*. Colorado, United States: Geol. Soc. Am.

Godet, A., Bodin, S., Föllmi, K. B., Vermeulen, J., Gardin, S., Fiet, N., et al. (2006). Evolution of the marine stable carbon-isotope record during the early cretaceous: A focus on the late hauterivian and barremian in the tethyan realm. *Earth Planet. Sci. Lett.* 242, 254–271. doi:10.1016/j.epsl.2005.12.011

Golterman, H. L. (2001). Phosphate release from anoxic sediments or `What did Mortimer really write? *Hydrobiologia* 450, 99–106. doi:10.1023/A:1017559903404

Golterman, H. L. (1995). The role of the ironhydroxide-phosphate-sulphide system in the phosphate exchange between sediments and overlying water. *Hydrobiologia* 297, 43–54. doi:10.1007/BF00033500

Gong, Z., van Hinsbergen, D. J. J., Vissers, R. L. M., and Dekkers, M. J. (2009). Early cretaceous syn-rotational extension in the organyà basin—New constraints on the palinspastic position of iberia during its rotation. *Tectonophysics* 473, 312–323. doi:10.1016/j.tecto.2009.03.003

Haq, B. U., Hardenbole, J., and Vail, P. R. (1988). "Mesozoic and Cenozoic chronostratigraphy and cycles of sea-level change," in *Sea-level changes: An integrated approach*. Editors C. K. Wilgus, B. S. Hastings, C. G. S. C Kendall, H. W. Posamentier, C. A. Ross, and J. C. Van Wagoner (McLean, United States: GeoScienceWorld), 71–108. Spec. Pub. Soc. Econ. Paleont. Miner. 42. doi:10.2110/pec.88.01.0071

Hatch, J. R., and Leventhal, J. S. (1992). Relationship between inferred redox potential of the depositional environment and geochemistry of the Upper Pennsylvanian (Missourian) Stark Shale Member of the Dennis Limestone, Wabaunsee County, Kansas, U.S.A. *U.S.A.* Chem. Geol. 99, 65–82. doi:10.1016/0009-2541(92)90031-Y

Head, I. M., Jones, D. M., and Röling, W. F. M. (2006). Marine microorganisms make a meal of oil. *Nat. Rev. Microbiol.* 4, 173–182. doi:10.1038/nrmicro1348

Hedges, J. I., Keil, R. G., and Benner, R. (1997). What happens to terrestrial organic matter in the ocean? *Org. Geochem.* 27, 195–212. doi:10.1016/S0146-6380(97)00066-1

Helz, G. R., Bura-Nakić, E., Mikac, N., and Ciglenečki, I. (2011). New model for molybdenum behavior in euxinic waters. *Chem. Geol.* 284, 323–332. doi:10.1016/j.chemgeo.2011.03.012

Helz, G. R., Miller, C. V., Charnock, J. M., Mosselmans, J. F. W., Pattrick, R. A. D., Garner, C. D., et al. (1996). Mechanism of molybdenum removal from the sea and its concentration in black shales: EXAFS evidence. *Geochimica Cosmochimica Acta* 60, 3631–3642. doi:10.1016/0016-7037(96)00195-0

Herdocia, C., and Maurrasse, F. J. R. (2022). Chemostratigraphic characteristics of trace elements, biomarkers, and clay mineralogy indicating environmental conditions within Aptian sediments of the Organyà Basin, North-East Spain, prior to the onset of OAE 1a. *Depositional Rec.* 8, 931–957. doi:10.1002/dep2.186

Herrle, J. O., Kößler, P., Friedrich, O., Erlenkeuser, H., and Hemleben, C. (2004). High-resolution carbon isotope records of the Aptian to Lower Albian from SE France and the Mazagan Plateau (DSDP Site 545): a stratigraphic tool for paleoceanographic and paleobiologic reconstruction. *Earth Planet. Sci. Lett.* 218, 149–161. doi:10.1016/S0012-821X(03)00646-0

Hetzel, A., Böttcher, M. E., Wortmann, U. G., and Brumsack, H.-J. (2009). Paleo-redox conditions during OAE 2 reflected in Demerara Rise sediment geochemistry (ODP Leg 207). *Palaeogeogr. Palaeoclimatol. Palaeoecol.* 273, 302–328. doi:10.1016/j.palaeo.2008.11.005

Hoffman, J., and Hower, J. (1979). "Clay Mineral Assemblages as Low Grade Metamorphic Geothermometers: Application to the Thrust Faulted Disturbed Belt of Montana, U.S.A," in *Aspects of diagenesis*. Editors P. M. Scholle and P. Schulger (McLean, United States: GeoScienceWorld), 55–79. R. Soc. Econo. Paleontol. Mineral. Spec. Pub. 26. doi:10.2110/pec.79.26.0055

Holtvoeth, J., Vogel, H., Wagner, B., and Wolff, G. A. (2010). Lipid biomarkers in Holocene and glacial sediments from ancient Lake Ohrid (Macedonia, Albania). *Biogeosciences* 7, 3473–3489. doi:10.5194/bg-7-3473-2010

Hower, J., Eslinger, E. V., Hower, M. E., and Perry, E. A. (1976). Mechanism of burial metamorphism of argillaceous sediment: 1. Mineralogical and chemical evidence. *Geol. Soc. Am. Bull.* 87, 725–737. doi:10.1130/0016-7606(1976)87<725:MOBMOA>2.0.CO;2

Hu, X., Li, J., Han, Z., and Li, Y. (2020). Two types of hyperthermal events in the Mesozoic-Cenozoic: Environmental impacts, biotic effects, and driving mechanisms. *Sci. China Earth Sci.* 63 (8), 1041–1058. doi:10.1007/s11430-019-9604-4

Hua, G., Yuansheng, D., Lian, Z., Jianghai, Y., Hu, H., Min, L., et al. (2013). Trace and rare Earth elemental geochemistry of carbonate succession in the Middle Gaoyuzhuang Formation, Pingquan Section: Implications for Early Mesoproterozoic Ocean redox conditions. *J.* Palaeogeogr. 2, 209–221. doi:10.3724/SP.J.1261.2013.00027

Huang, Y., Yang, G., Wang, C., and Wu, H. (2012). The stabilisation of the long-term Cretaceous greenhouse climate: Contribution from the semi-periodical burial of phosphorus in the ocean. *Cretac. Res.* 38, 7–15. doi:10.1016/j.cretres.2012.04.005

Huber, B. T., Hodell, D. A., and Hamilton, C. P. (1995). Middle–Late Cretaceous climate of the southern high latitudes: stable isotopic evidence for minimal equator-to-pole thermal gradients. *Geol. Soc. Am. Bull.* 107, 1164–1191. doi:10.1130/0016-7606(1995)107<1164:MLCCOT>2.3.CO;2

Huber, B. T., MacLeod, K. G., Watkins, D. K., and Coffin, M. F. (2018). The rise and fall of the Cretaceous Hot Greenhouse climate. *Glob. Planet. Change* 167, 1–23. doi:10.1016/j.gloplacha.2018.04.004

Husinec, A., Harman, C. A., Regan, S. P., Mosher, D. A., Sweeney, R. J., and Read, J. F. (2012). Sequence development influenced by intermittent cooling events in the Cretaceous Aptian greenhouse, Adriatic platform, Croatia. *AAPG Bull.* 96, 2215–2244. doi:10.1306/05161211175

Jenkyns, H. C. (1995). Carbon-isotope stratigraphy and paleoceanographic significance of the Lower Cretaceous shallow-water carbonates of Resolution Guyot, Mid-Pacific Mountains. *Proc. Ocean. Drill. Program Sci. Results* 143, 99–108.

Johnson, R. W., and Calder, J. A. (1973). Early diagenesis of fatty acids and hydrocarbons in a salt marsh environment. *Geochimica Cosmochimica Acta* 37, 1943–1955. doi:10.1016/0016-7037(73)90150-6

Jones, B., and Manning, D. A. C. (1994). Comparison of geochemical indices used for the interpretation of palaeoredox conditions in ancient mudstones. *Chem. Geol.* 111 (1), 111–129. doi:10.1016/0009-2541(94)90085-X

Keil, R. G., and Mayer, L. M. (2014). "12.12 - Mineral Matrices and Organic Matter," in *Treatise on geochemistry*. Editors H. D. Holland and K. K. Turekian Second Edition (Oxford: Elsevier), 337–359.

Kossovskaya, A. G., and Drits, V. A. (1970). The Variability of Micaceous Minerals in Sedimentary Rocks. *Sedimentology* 15, 83–101. doi:10.1111/j.1365-3091.1970.tb00207.x

Koutsoukos, E. A. M., Mello, M. R., and de Azambuja Filho, N. C. (1991b). Micropalaeontological and geochemical evidence of mid-Cretaceous dysoxic-anoxic palaeoenvironments in the Sergipe Basin, northeastern Brazil. *Geol. Soc. Lond. Spec. Publ.* 58, 427–447. doi:10.1144/GSL.SP.1991.058.01.27

Koutsoukos, E. A. M., Mello, M. R., De Azambuja Filho, N. C., Hart, M. B., and Maxwell, J. R. (1991a). The Upper Aptian–Albian Succession of the Sergipe Basin, Brazil: An Integrated Paleoenvironmental Assessment1. *AAPG Bull.* 75, 479–498. doi:10.1306/0C9B2817-1710-11D7-8645000102C1865D

Kuhnt, W., Holbourn, A., and Moullade, M. (2011). Transient global cooling at the onset of early Aptian oceanic anoxic event (OAE) 1a. *Geology* 39, 323–326. doi:10.1130/G31554.1

Kuhnt, W., Moullade, M., Masse, J.-P., and Erlenkeuser, H. (1998). Carbon isotope stratigraphy of the lower Aptian historical stratotype at Cassis-La Bédoule (SE France). *Géologie Méditerranéenne* 25, 63–79. doi:10.3406/geolm.1998.1625

Larson, R. L., and Erba, E. (1999). Onset of the Mid-Cretaceous greenhouse in the Barremian-Aptian: Igneous events and the biological, sedimentary, and geochemical responses. *Paleoceanography* 14, 663–678. doi:10.1029/1999PA900040

Larson, R. L. (1991). Geological consequences of superplumes. *Geology* 19, 963–966. doi:10.1130/0091-7613(1991)019<0963:GCOS>2.3.CO;2

Leckie, R. M., Bralower, T. J., and Cashman, R. (2002). Oceanic anoxic events and plankton evolution: Biotic response to tectonic forcing during the mid-Cretaceous. *Paleoceanography* 17, 13-1–13-29. doi:10.1029/2001PA000623

Léonide, P., Floquet, M., Durlet, C., Baudin, F., Pittet, B., and Lécuyer, C. (2012). Drowning of a carbonate platform as a precursor stage of the Early Toarcian global anoxic event (Southern Provence sub-Basin, South-east France). *Sedimentology* 59, 156–184. doi:10.1111/j.1365-3091.2010.01221.x

Li, Y.-X., Bralower, T. J., Montañez, I. P., Osleger, D. A., Arthur, M. A., Bice, D. M., et al. (2008). Toward an orbital chronology for the early Aptian Oceanic Anoxic Event (OAE1a, ~120 Ma). *Earth Planet. Sci. Lett.* 271, 88–100. doi:10.1016/j.epsl.2008.03.055

Lijmbach, W. M. (1975). "On the Origin of Petroleum," in *Proceedings of the 9th world petroleum congress* (London: Applied science publishers), 357–369.

Lini, A., Weissert, H., and Erba, E. (1992). The Valanginian carbon isotope event: a first episode of greenhouse climate conditions during the Cretaceous. *Terra nova.* 4, 374–384. doi:10.1111/j.1365-3121.1992.tb00826.x

Lorenzen, J., Kuhnt, W., Holbourn, A., Flögel, S., Moullade, M., and Tronchetti, G. (2013). A new sediment core from the Bedoulian (Lower Aptian) stratotype at

Roquefort–La Bédoule, SE France. *Cretac. Res.* 39, 6–16. doi:10.1016/j.cretres.2012.03.019

Martin-Chivelet, J., Beràstegui, X., Rosales, I., Vilas, L., Vera, J. A., Caus, E., et al. (2002). in *Cretaceous" in* the Geology of Spain. Editors W. Gibbons and T. Moreno (London: The Geological Society), 255–292.

Martiny, A. C., Lomas, M. W., Fu, W., Boyd, P. W., Chen, Y. l. L., Cutter, G. A., et al. (2019). Biogeochemical controls of surface ocean phosphate. *Sci. Adv.* 5, eaax0341. doi:10.1126/sciadv.aax0341

Masse, J. P., and Machhour, L. (1998). La matière organique dans la série du stratotype historique de l'Aptien inférieur dans la région de Cassis-La Bédoule (SE France). *Géologie Méditerranéenne* 25 (3), 55–62. doi:10.3406/geolm.1998.1624

Maurrasse, F. J-M. R., and Ponton, C. (2005). "Aptian deposits in southeastern France and northeastern Mexico: Implications concerning paleoclimatic conditions: Scientific Program and Abstracts," in *7th international symposium on the cretaceous* (Switzerland: Neuchatel), 137.

McIntosh, J. A., Tabor, N. J., and Rosenau, N. A. (2021). Mixed-Layer Illite-Smectite in Pennsylvanian-Aged Paleosols: Assessing Sources of Illitization in the Illinois Basin. *Minerals* 11, 108. doi:10.3390/min11020108

Mencos, J., Muñoz, J. A., and Hardy, S. (2010). 3D kinematics of the Sant Corneli anticline: insights from structural reconstruction and forward modelling. *Trab. Geol.* 30, 75–80.

Menegatti, A. P., Weissert, H., Brown, R. S., Tyson, R. V., Farrimond, P., Strasser, A., et al. (1998). High-resolution δ13C stratigraphy through the early Aptian "Livello Selli" of the Alpine Tethys. *Paleoceanography* 13, 530–545. doi:10.1029/98PA01793

Meunier, A. (2005). *Clays. Springer-verlag berlin heidelberg*. New York: Springer Berlin Heidelberg, 486. 3-540-21667-7.

Michalík, J., Soták, J., Lintnerová, O., Halásová, E., Bąk, M., Skupien, P., et al. (2008). The stratigraphic and paleoenvironmental setting of Aptian OAE black shale deposits in the Pieniny Klippen Belt, Slovak Western Carpathians. *Cretac. Res.* 29, 871–892. doi:10.1016/j.cretres.2008.05.005

Millán, M. I., Weissert, H. J., Fernández-Mendiola, P. A., and García-Mondéjar, J. (2009). Impact of Early Aptian carbon cycle perturbations on evolution of a marine shelf system in the Basque-Cantabrian Basin (Aralar, N Spain). *Earth Planet. Sci. Lett.* 287, 392–401. doi:10.1016/j.epsl.2009.08.023

Moore, D. M., and Reynolds, R. C., Jr (1989). *X-Ray diffraction and the identification and analysis of clay minerals*. New York: Oxford University Press, 378.

Moosavizadeh, M. A., Mahboubi, A., Moussavi-Harami, R., and Kavoosi, M. A. (2014). Early Aptian oceanic anoxic event (OAE 1a) in Northeastern Arabian Plate setting: an example from Dariyan Formation in Zagros fold–trust belt, SE Iran. *Arab. J. Geosci.* 7, 4745–4756. doi:10.1007/s12517-013-1025-z

Moreno-Bedmar, J. A. (2010). *Ammonits de l'Aptià inferior de la península Ibèrica. Biostratigrafia i aportacions a l'estudi del Ocean. Anoxic Event 1a*. Barcelona, Spain]: University of Barcelona, 331. [dissertation].

Moreno-Bedmar, J. A., Company, M., Bover-Arnal, T., Salas, R., Delanoy, G., Martínez, R., et al. (2009). Biostratigraphic characterization by means of ammonoids of the lower Aptian Oceanic Anoxic Event (OAE 1a) in the eastern Iberian Chain (Maestrat Basin, Eastern Spain). *Cretac. Res.* 30, 864–872. doi:10.1016/j.cretres.2009.02.004

Morford, J. L., and Emerson, S. (1999). The geochemistry of redox sensitive trace metals in sediments. *Geochimica Cosmochimica Acta* 63, 1735–1750. doi:10.1016/S0016-7037(99)00126-X

Morford, J. L., Russell, A. D., and Emerson, S. (2001). Trace metal evidence for changes in the redox environment associated with the transition from terrigenous clay to diatomaceous sediment, Saanich Inlet, BC. *Mar. Geol.* 174 (1), 355–369. doi:10.1016/S0025-3227(00)00160-2

Muñoz, M., Vidal, O., Marcaillou, C., Pascarelli, S., Mathon, O., and Farges, F. (2013). Iron oxidation state in phyllosilicate single crystals using Fe-K pre-edge and XANES spectroscopy: Effects of the linear polarization of the synchrotron X-ray beam. *Am. Mineralogist* 98, 1187–1197. doi:10.2138/am.2013.4289

Murphy, A. E., Sageman, B. B., Hollander, D. J., Lyons, T. W., and Brett, C. E. (2000). Black shale deposition and faunal overturn in the Devonian Appalachian Basin: Clastic starvation, seasonal water-column mixing, and efficient biolimiting nutrient recycling. *Paleoceanography* 15, 280–291. doi:10.1029/1999PA000445

Mutterlose, J., and Böckel, B. (1998). The Barremian–Aptian interval in NW Germany: A review. *Cretac. Res.* 19, 539–568. doi:10.1006/cres.1998.0119

Najarro, M., Rosales, I., and Martín-Chivelet, J. (2011a). Major palaeoenvironmental perturbation in an early Aptian carbonate platform: Prelude of the oceanic anoxic event 1a? *Sediment. Geol.* 235, 50–71. doi:10.1016/j.sedgeo.2010.03.011

Najarro, M., Rosales, I., Moreno-Bedmar, J. A., de Gea, G. A., Barrón, E., Company, M., et al. (2011b). High-resolution chemo-and biostratigraphic records of the Early Aptian oceanic anoxic event in Cantabria (N Spain): Palaeoceanographic and palaeoclimatic implications. *Palaeogeogr. Palaeoclimatol. Palaeoecol.* 299, 137–158. doi:10.1016/j.palaeo.2010.10.042

Nishimura, M., and Baker, E. W. (1986). Possible origin of with a remarkable even-to-odd predominance in recent marine sediments. *Geochimica Cosmochimica Acta* 50, 299–305. doi:10.1016/0016-7037(86)90178-X

Pardue, J. W., Scalan, R. S., Van Baalen, C., and Parker, P. L. (1976). Maximum carbon isotope fractionation in photosynthesis by blue-green algae and a green alga. *Geochimica Cosmochimica Acta* 40, 309–312. doi:10.1016/0016-7037(76)90208-8

Pattan, J. N., and Pearce, N. J. G. (2009). Bottom water oxygenation history in southeastern Arabian Sea during the past 140ka: Results from redox-sensitive elements. *Palaeogeogr. Palaeoclimatol. Palaeoecol.* 280, 396–405. doi:10.1016/j.palaeo.2009.06.027

Pauly, S., Mutterlose, J., and Wray, D. S. (2013). Palaeoceanography of Lower Cretaceous (Barremian–Lower Aptian) black shales from northwest Germany evidenced by calcareous nannofossils and geochemistry. *Cretac. Res.* 42, 28–43. doi:10.1016/j.cretres.2013.01.001

Pearson, K. (1896). Mathematical Contributions to the Theory of Evolution. On a Form of Spurious Correlation Which May Arise When Indices Are Used in the Measurement of Organs. *Proc. R. Soc. Lond.* 60, 489–498. doi:10.1098/rspl.1896.0076

Peters, K. E., Walters, C. C., and Moldowan, J. M. (2005). *The biomarker guide: I: Biomarkers and isotopes in the environment and human history*. Cambridge, UK: Cambridge University Press. doi:10.1016/0146-6380(93)90028-A

Peters, K. E., Walters, C. C., and Moldowan, J. M. (2007). *The biomarker guide: II, biomarkers and isotopes in petroleum systems and Earth history*. Cambridge, UK: Cambridge University Press, 475–1155.

Pinck, L. A., and Allison, F. E. (1951). Resistance of a Protein-Montmorillonite Complex to Decomposition by Soil Microorganisms. *Science* 114, 130–131. doi:10.1126/science.114.2953.130

Ponton, C., West, A. J., Feakins, S. J., and Galy, V. (2014). Leaf wax biomarkers in transit record river catchment composition. *Geophys. Res. Lett.* 41, 6420–6427. doi:10.1002/2014GL061328

Ponton Guerrero, C. (2006). Barremian-Aptian depositional environments and their sediments: The Mexican versus the Provencal (France) platforms, paleoenvironmental implications. Miami, USA: Florida International University, 113. [thesis].

Porrenga, D. H. (1968). Non-marine glauconitic illite in the Lower Oligocene of Aardebrug, Belgium. *Clay Miner.* 7 (4), 421–430. doi:10.1180/claymin.1968.007.4.05

Prietzel, J., Thieme, J., Eusterhues, K., and Eichert, D. (2007). Iron speciation in soils and soil aggregates by synchrotron-based X-ray microspectroscopy (XANES,μ-XANES). *Eur. J. Soil Sci.* 58, 1027–1041. doi:10.1111/j.1365-2389.2006.00882.x

Puigdefàbregas, C., and Souquet, P. (1986). Tecto-sedimentary cycles and depositional sequences of the Mesozoic and Tertiary from the Pyrenees. *Tectonophysics* 129, 173–203. doi:10.1016/0040-1951(86)90251-9

Puttonen, I., Kohonen, T., and Mattila, J. (2016). Factors controlling phosphorus release from sediments in coastal archipelago areas. *Mar. Pollut. Bull.* 108, 77–86. doi:10.1016/j.marpolbul.2016.04.059

Quijano, M. L., Castro, J. M., Pancost, R. D., de Gea, G. A., Najarro, M., Aguado, R., et al. (2012). Organic geochemistry, stable isotopes, and facies analysis of the Early Aptian OAE—New records from Spain (Western Tethys). *Palaeogeogr. Palaeoclimatol. Palaeoecol.* 365-366, 276–293. doi:10.1016/j.palaeo.2012.09.033

Rat, P. (1988). The Basque-Cantabrian Basin between the Iberian and European plates, some facts but still many problems. *Rev. Soc. Geol. España* 1 (3 -4), 327–348.

Ravelo, A. C., and Fairbanks, R. G. (1995). Carbon isotopic fractionation in multiple species of planktonic foraminifera from core-tops in the tropical Atlantic. *J. Foraminifer. Res.* 25, 53–74. doi:10.2113/gsjfr.25.1.53

Rimmer, S. M. (2004). Geochemical paleoredox indicators in Devonian–Mississippian black shales, central Appalachian Basin (USA). *Chem. Geol.* 206, 373–391. doi:10.1016/j.chemgeo.2003.12.029

Roban, R.-D., and Melinte-Dobrinescu, M. C. (2012). Lower Cretaceous lithofacies of the black shales rich Audia Formation, Tarcău Nappe, Eastern Carpathians: Genetic significance and sedimentary palaeoenvironments. *Cretac. Res.* 38, 52–67. doi:10.1016/j.cretres.2012.06.002

Ruffell, A., McKinley, J. M., and Worden, R. H. (2002). Comparison of clay mineral stratigraphy to other proxy palaeoclimate indicators in the Mesozoic of NW Europe. *Philosophical Trans. R. Soc. Lond. Ser. A Math. Phys. Eng. Sci.* 360, 675–693. doi:10.1098/rsta.2001.0961

Sage, R. F. (2004). The evolution of C4 photosynthesis. *New Phytol.* 161, 341–370. doi:10.1111/j.1469-8137.2004.00974.x

Sanchez-Hernandez, Y., and Maurrasse, F. J-M. R. (2014). Geochemical characterization and redox signals from the latest Barremian to the earliest Aptian in a restricted marine basin: El Pui section, Organyà Basin, south-central Pyrenees. *Chem. Geol.* 372, 12–31. doi:10.1016/j.chemgeo.2014.02.011

Sanchez-Hernandez, Y., Maurrasse, F. J-M. R., Melinte-Dobrinescu, M. C., He, D., and Butler, S. K. (2014). Assessing the factors controlling high sedimentation rates from the latest Barremian–earliest Aptian in the hemipelagic setting of the restricted Organyà Basin, NE Spain. *Cretac. Res.* 51, 1–21. doi:10.1016/J.CRETRES.2014.05.010

Sanchez-Hernandez, Y., and Maurrasse, F. J-M. R. (2016). The influence of regional factors in the expression of oceanic anoxic event 1a (OAE1a) in the semi-restricted Organyà Basin, south-central Pyrenees, Spain. *Palaeogeogr. Palaeoclimatol. Palaeoecol.* 441, 582–598. doi:10.1016/J.PALAEO.2015.06.031

Sanguësa, F. J., Arostegui, J., and Suarez-Ruiz, I. (2000). Distribution and origin of clay minerals in the Lower Cretaceous of the Alava Block (Basque-Cantabrian Basin, Spain). *Clay Min.* 35, 393–410. doi:10.1180/000985500546864

Scalan, E. S., and Smith, J. E. (1970). An improved measure of the odd even predominance in the normal alkanes of sediment extracts and petroleum. *Geochimica Cosmochimica Acta* 34, 611–620. doi:10.1016/0016-7037(70)90019-0

Scarparo Cunha, A. A., and Koutsoukos, E. A. M. (1998). Calcareous nannofossils and planktic foraminifers in the upper Aptian of the Sergipe Basin, northeastern Brazil: palaeoecological inferences. *Palaeogeogr. Palaeoclimatol. Palaeoecol.* 142, 175–184. doi:10.1016/S0031-0182(98)00065-0

Schlagintweit, F., Rosales, I., and Najarro, M. (2016). Glomospirella cantabrica n. sp., and other benthic foraminifera from Lower Cretaceous Urgonian-type carbonates of Cantabria, Spain: Biostratigraphic implications. *Geol. Acta* 14 (2), 113–138. doi:10.1344/GeologicaActa2016.14.2.3

Schlanger, S. O., and Jenkyns, H. C. (1976). Cretaceous oceanic anoxic events: causes and consequences. *Geol. Mijnb.* 55, 179–184.

Scholle, P. A., and Arthur, M. A. (1980). Carbon Isotope Fluctuations in Cretaceous Pelagic Limestones: Potential Stratigraphic and Petroleum Exploration Tool. *AAPG Bull.* 64, 67–87. doi:10.1306/2F91892D-16CE-11D7-8645000102C1865D

Scholz, F., McManus, J., and Sommer, S. (2013). The manganese and iron shuttle in a modern euxinic basin and implications for molybdenum cycling at euxinic ocean margins. *Chem. Geol.* 355, 56–68. doi:10.1016/j.chemgeo.2013.07.006

Scott, C. C. H. (1992). Clay mineralogy of the Upper Cretaceous Mancos Shale near Mesa Verde National Park, Southwestern Colorado: Clues to the paleoceanography of the Western Interior Seaway. Massachusetts, United States: University of Massachusetts, 191. Thesis.

Scott, C., Lyons, T. W., Bekker, A., Shen, Y., Poulton, S. W., Chu, X., et al. (2008). Tracing the stepwise oxygenation of the Proterozoic Ocean. *Nature* 452, 456–459. doi:10.1038/nature06811

Shanmugam, G. (1985). Significance of Coniferous Rain Forests and Related Organic Matter in Generating Commercial Quantities of Oil, Gippsland Basin, Australia. *AAPG Bull.* 69 (8), 1241–1254. doi:10.1306/AD462BC3-16F7-11D7-8645000102C1865D

Sheldon, N. D., and Tabor, N. J. (2009). Quantitative paleoenvironmental and paleoclimatic reconstruction using paleosols. *Earth-Science Rev.* 95, 1–52. doi:10.1016/j.earscirev.2009.03.004

Shields, G. A., and Mills, B. J. W. (2017). Tectonic controls on the long-term carbon isotope mass balance. *Proc. Natl. Acad. Sci.* 114, 4318–4323. doi:10.1073/pnas.1614506114

Siebert, C., McManus, J., Bice, A., Poulson, R., and Berelson, W. M. (2006). Molybdenum isotope signatures in continental margin marine sediments. *Earth Planet. Sci. Lett.* 241, 723–733. doi:10.1016/j.epsl.2005.11.010

Simonnin, P., Song, D., Alexandrov, V., Bylaska, E. J., and Rosso, K. J. (2017). "Modeling electron transfer in iron-bearing phyllosilicate minerals," in *Computational modeling in clay mineralogy, Chap. 5*. Editor C. I. Saint-Diaz (Bengaluru, Karnataka: Digilabs), 141–174. AIPEA Educational Series, Publication No. 3.

Sinton, C. W., and Duncan, R. A. (1997). Potential links between ocean plateau volcanism and global ocean anoxia at the Cenomanian-Turonian boundary. *Econ. Geol.* 92, 836–842. doi:10.2113/gsecongeo.92.7-8.836

Socorro, J., Maurrasse, F. J-M. R., and Sanchez-Hernandez, Y. (2017). Characterization of the negative carbon isotope shift in segment C2, its global implications as a harbinger of OAE1a. *Sci. China Earth Sci.* 60, 30–43. doi:10.1007/s1143-0-016-0092-5

Socorro, J., and Maurrasse, F. J-M. R. (2019). Continuous accumulation of organic matter-rich sediments associated with Oceanic Anoxic Event 1a in the El Pujal section, Organyà Basin, Catalunyà Spain and its relation to episodic dysoxia. *Cretac. Res.* 95, 225–251. doi:10.1016/J.CRETRES.2018.11.009

Socorro, J., and Maurrasse, F. J.-M. R. (2022). Demise of Organic Matter–Rich Facies and Changing Paleoenvironmental Conditions Associated with the End of Carbon Isotope Segment C5 of Oceanic Anoxic Event 1a in the North and Northeastern Iberian Peninsula. *J. Geol.* 130, 133–170. doi:10.1086/718834

Socorro, J., and Maurrasse, F. J. R. (2020). Regional palaeoenvironmental influence on organic matter sequestration and characteristics of carbon isotope segment C5 in a hemipelagic sequence, Organyà Basin, northeast Spain. *Depositional Rec.* 6, 552–580. doi:10.1002/dep2.111

Sohrin, Y., Fujishima, Y., Ueda, K., Akiyama, S., Mori, K., Hasegawa, H., et al. (1998). Dissolved niobium and tantalum in the North Pacific. *Geophys. Res. Lett.* 25, 999–1002. doi:10.1029/98GL00646

Swart, P. K., Blättler, C. L., Nakakuni, M., Mackenzie, G. J., Betzler, C., Eberli, G. P., et al. (2019). Cyclic anoxia and organic rich carbonate sediments within a drowned carbonate platform linked to Antarctic ice volume changes: Late Oligocene-early Miocene Maldives. *Earth Planet. Sci. Lett.* 521 (1-13), 1–13. ISSN 0012-821X. doi:10.1016/j.epsl.2019.05.019

Tarduno, J. A., Sliter, W. V., Kroenke, L., Leckie, M., Mayer, H., Mahoney, J. J., et al. (1991). Rapid Formation of Ontong Java Plateau by Aptian Mantle Plume Volcanism. *Science* 254, 399–403. doi:10.1126/science.254.5030.399

Tatsumi, Y., Shinjoe, H., Ishizuka, H., Sager, W. W., and Klaus, A. (1998). Geochemical evidence for a mid-Cretaceous superplume. *Geology* 26, 151–154. doi:10.1130/0091-7613(1998)026<0151:GEFAMC>2.3.CO;2

Taylor, G. T., Iabichella, M., Ho, T.-Y., Scranton, M. I., Thunell, R. C., Muller-Karger, F., et al. (2001). Chemoautotrophy in the redox transition zone of the Cariaco Basin: A significant midwater source of organic carbon production. *Limnol. Oceanogr.* 46, 148–163. doi:10.4319/lo.2001.46.1.0148

Tejada, M. L. G., Suzuki, K., Kuroda, J., Coccioni, R., Mahoney, J. J., Ohkouchi, N., et al. (2009). Ontong Java Plateau eruption as a trigger for the early Aptian oceanic anoxic event. *Geology* 37, 855–858. doi:10.1130/G25763A.1

Tribovillard, N., Ramdani, A., and Trentesaux, A. (2005). "Controls on Organic Accumulation in Upper Jurassic Shales of Northwestern Europe as Inferred from Trace-Metal Geochemistry," in *The deposition of organic-carbon-rich sediments: Models, mechanisms, and consequences*. Editor N. Harris (Tulsa, Oklahoma: SEPM Special Publication), 145–164.

Tribovillard, N., Riboulleau, A., Lyons, T., and Baudin, F. (2004). Enhanced trapping of molybdenum by sulfurized marine organic matter of marine origin in Mesozoic limestones and shales. *Chem. Geol.* 213 (4), 385–401. doi:10.1016/j.chemgeo.2004.08.011

Turekian, K. K., and Wedepohl, K. H. (1961). Distribution of the Elements in Some Major Units of the Earth's Crust. *GSA Bull.* 72, 175–192. doi:10.1130/0016-7606(1961)72[175:DOTEIS]2.0.CO;2

Van der Weijden, C. H. (2002). Pitfalls of normalization of marine geochemical data using a common divisor. *Mar. Geol.* 184, 167–187. doi:10.1016/S0025-3227(01)00297-3

Wagreich, M. (2012). "OAE 3" – regional Atlantic organic carbon burial during the Coniacian–Santonian. *Clim. Past.* 8, 1447–1455. doi:10.5194/cp-8-1447-2012

Weaver, C. E. (1956). A discussion on the origin of clay minerals in sedimentary rocks. *Clays Clay Minerals* 5, 159–173. doi:10.1346/CCMN.1956.0050113

Weaver, C. E. (1989). *Developments in sedimentology:* Clays, muds, and shales. Amsterdam, Netherlands: Elsevier.

Wedepohl, K. H. (1991). "The composition of the upper earth's crust and the natural cycles of selected metals. Metals in natural raw materials. Natural Resources," in *Metals and their compounds in the environment*. Editor E. Merian. Weinheim (Vancouver, Canada: VCH), 3–17.

Wei, Q., Yuan, Y., Song, S., Zhao, Y., Sun, J., Li, C., et al. (2022). Spatial variability of hypoxia and coupled physical-biogeochemical controls off the Changjiang (Yangtze River) Estuary in summer. *Front. Mar. Sci.* 9, 987368. doi:10.3389/fmars.2022.987368

White, W. M. (2013). *Geochemistry*. Hoboken, USA: Wiley-Blackwell. 111 River Street, 660.

Wilmsen, M. (2005). Stratigraphy and biofacies of the Lower Aptian of Cuchía (Cantabria, northern Spain). *J. Iber. Geol.* 31, 253–275.

Wilson, M. J. (1999). The origin and formation of clay minerals in soils: past, present and future perspectives. *Clay Min.* 34, 7–25. doi:10.1180/000985599545957

Yilmaz, I. O. (2008). Cretaceous Pelagic Red Beds and Black Shales (Aptian-Santonian), NW Turkey: Global Oceanic Anoxic and Oxic Events. *Turk. J. Earth Sci.* 17, 263–296.

Zhang, L., Xiao, D., Lu, S., Jiang, S., and Lu, S. (2019). Effect of sedimentary environment on the formation of organic-rich marine shale: Insights from major/trace elements and shale composition. *Int. J. Coal Geol.* 204, 34–50. doi:10.1016/j.coal.2019.01.014

Zhang, X., Zhang, G., and Sha, J. (2016). Lacustrine sedimentary record of early Aptian carbon cycle perturbation in Western Liaoning, China. *Cretac. Res.* 62, 122–129. doi:10.1016/J.CRETRES.2015.10.001

Zhao, L., Hong, H., Liu, J., Fang, Q., Yao, Y., Tan, W., et al. (2018). Assessing the utility of visible-to-shortwave infrared reflectance spectroscopy for analysis of soil weathering intensity and paleoclimate reconstruction. *Palaeogeogr. Palaeoclimatol. Palaeoecol.* 512, 80–94. doi:10.1016/j.palaeo.2017.07.007